Article

Cell

Identification of a Brainstem Circuit Controlling Feeding

Graphical Abstract

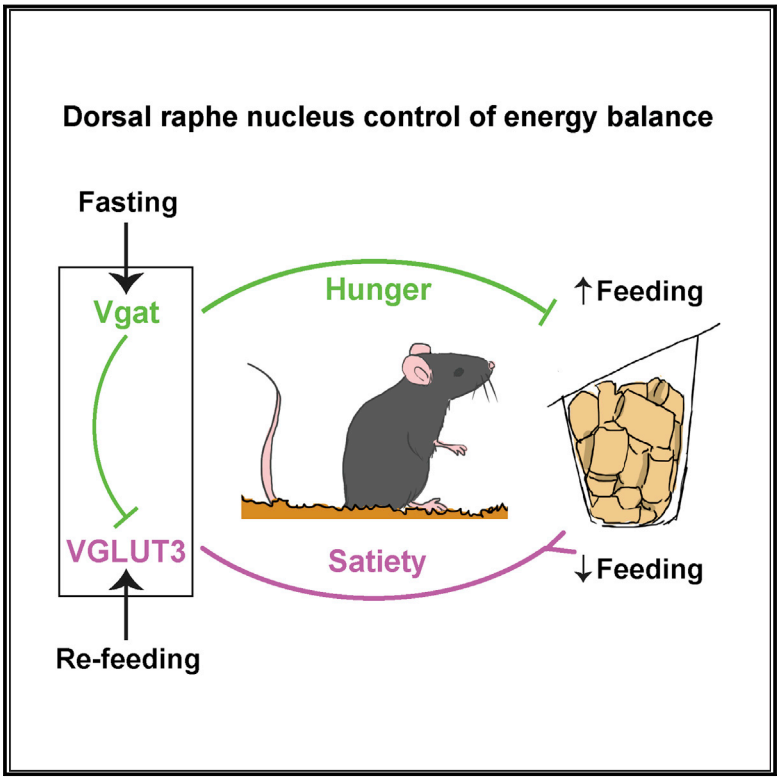

Authors

Alexander R. Nectow, Marc Schneeberger, Hongxing Zhang, ..., Marc Tessier-Lavigne, Ming-Hu Han, Jeffrey M. Friedman

Correspondence

anectow@princeton.edu (A.R.N.), friedj@rockefeller.edu (J.M.F.)

In Brief

A combination of brain mapping and molecular pharmacology approaches identifies specific neurons in the dorsal raphe nucleus as being important regulators of feeding behavior.

Highlights

- Fasting activates DRN^{Vgat} neurons; re-feeding activates DRN^{VGLUT3} neurons
- Activation of DRN^{Vgat} neurons increases and DRN^{VGLUT3} suppresses feeding
- Inhibiting DRN^{Vgat} neurons in obese mice reduces food intake and body weight
- DRN neurons can be regulated pharmacologically to drive changes in food intake

Data Resources

GSE87890

Nectow et al., 2017, Cell *170*, 429–442
July 27, 2017
http://dx.doi.org/10.1016/j.cell.2017.06.045

CellPress

Cell

Identification of a Brainstem Circuit Controlling Feeding

Alexander R. Nectow,[1,6,7,*] Marc Schneeberger,[1,7] Hongxing Zhang,[2,7] Bianca C. Field,[1] Nicolas Renier,[3,4] Estefania Azevedo,[1] Bindiben Patel,[6] Yupu Liang,[5] Siddhartha Mitra,[5] Marc Tessier-Lavigne,[3] Ming-Hu Han,[2] and Jeffrey M. Friedman[1,8,*]

[1]Laboratory of Molecular Genetics, Howard Hughes Medical Institute, The Rockefeller University, New York, NY 10065, USA
[2]Department of Pharmacological Sciences, Friedman Brain Institute, Icahn School of Medicine at Mount Sinai, New York, NY 10029, USA
[3]Laboratory of Brain Development and Repair, The Rockefeller University, New York, NY 10065, USA
[4]ICM, Brain and Spine Institute, Hopital de la Pitie-Salpetriere, Paris 75013, France
[5]Hospital Informatics, The Rockefeller University, New York, NY 10065, USA
[6]Princeton Neuroscience Institute, Princeton University, Princeton, NJ 08544, USA
[7]These authors contributed equally
[8]Lead Contact
*Correspondence: anectow@princeton.edu (A.R.N.), friedj@rockefeller.edu (J.M.F.)
http://dx.doi.org/10.1016/j.cell.2017.06.045

SUMMARY

Hunger, driven by negative energy balance, elicits the search for and consumption of food. While this response is in part mediated by neurons in the hypothalamus, the role of specific cell types in other brain regions is less well defined. Here, we show that neurons in the dorsal raphe nucleus, expressing vesicular transporters for GABA or glutamate (hereafter, DRN^{Vgat} and DRN^{VGLUT3} neurons), are reciprocally activated by changes in energy balance and that modulating their activity has opposite effects on feeding—DRN^{Vgat} neurons increase, whereas DRN^{VGLUT3} neurons suppress, food intake. Furthermore, modulation of these neurons in obese (*ob*/*ob*) mice suppresses food intake and body weight and normalizes locomotor activity. Finally, using molecular profiling, we identify druggable targets in these neurons and show that local infusion of agonists for specific receptors on these neurons has potent effects on feeding. These data establish the DRN as an important node controlling energy balance.

INTRODUCTION

The regulation of nutrient intake is essential for survival in all organisms. In mammals, energy balance is tightly regulated and changes in metabolic state result in compensatory effects on food intake and energy expenditure. This homeostatic control mechanism is maintained by neurons in several brain regions, including the hypothalamus (Aponte et al., 2011; Jennings et al., 2015; Krashes et al., 2014) and other brain areas such as the extended amygdala (Jennings et al., 2013) and brainstem (Carter et al., 2013). These neurons respond to nutritional and humoral signals, such as leptin, which circulates in proportion to body fat content. Obesity is associated with high levels of leptin and insensitivity to its exogenous administration. Thus, one approach to treat obesity would be to modulate the activity of neural populations that regulate feeding independent of leptin signaling. Here, we identify two cell types within the dorsal raphe nucleus (DRN) that potently regulate food intake and locomotor activity in wild-type and leptin-deficient *ob*/*ob* mice.

The DRN is a brainstem nucleus in the dorsal midbrain that has been implicated in the control of food intake, although the neurons responsible for this effect have not been identified. The DRN is located directly beneath the cerebral aqueduct and has reciprocal connections with numerous hypothalamic nuclei known to control feeding, such as the lateral hypothalamus (LHA) and paraventricular hypothalamus (Garfield et al., 2015; Larsen et al., 1996; Petrovický et al., 1981; Weissbourd et al., 2014). Previous chemogenetic (Stachniak et al., 2014), pharmacological (Bendotti et al., 1986; Carlini et al., 2004; Fletcher and Davies, 1990), and electrophysiological (Veasey et al., 1997) studies probing the function of this entire nucleus in a non-cell-specific manner have also suggested a role for the DRN in controlling food intake and other behaviors.

The DRN is comprised of at least four principal cell types, releasing serotonin, glutamate, GABA, and/or dopamine, with additional cell populations expressing overlapping sets of these and other marker genes (Hioki et al., 2010; Okaty et al., 2015). Subsets of DRN neurons have been evaluated for their role in controlling social- (Matthews et al., 2016; Okaty et al., 2015), reward- (Liu et al., 2014; McDevitt et al., 2014), pain- (Li et al., 2016), and depression-related (Challis et al., 2013; Warden et al., 2012) behaviors. However, a direct role for specific DRN cell types in controlling feeding or its associated behaviors has not been established.

In the current work, we use a combination of approaches to establish a role for DRN neurons expressing the vesicular transporters Vgat (*Slc32a1*) and VGLUT3 (*Slc17a8*) in controlling food intake and body weight. We report that these DRN^{Vgat} and DRN^{VGLUT3} neurons are molecularly and anatomically distinct, and modulating their activity reciprocally regulates food intake. This effect is also demonstrated in obese (*ob*/*ob*) mice. Finally, we show that pharmacological manipulation of receptors on

these DRN neurons can exert bidirectional control of food intake. Together, these studies establish an important role for the DRN in regulating feeding and provide a potential pharmacological approach for modulating food intake and body weight.

RESULTS

Whole Brain Activity Mapping in Fed and Fasted Mice

The CNS is responsive to alterations in metabolic state, resulting in brain-wide changes in neural activity. We reasoned that some of the sites that are sensitive to changes in energy balance might play an active role in controlling feeding. We thus set out to identify anatomic sites whose activity is altered in fed versus fasted mice in an unbiased manner by generating averaged maps of Fos-positive (Fos^+) neurons in whole brain using iDISCO+. This approach allows analysis of intact, whole brain through tissue clearing (Renier et al., 2014, 2016). After whole-mount immunostaining for Fos and brain clearing, cell detection and registration were performed using ClearMap (Renier et al., 2016) (Figure 1A). Consistent with prior data, 3D automated mapping of cells expressing Fos using the Allen Brain Atlas annotation revealed a high density of Fos^+ cells in the arcuate nucleus of the hypothalamus (ARC) in fasted animals (Figure 1B). The ARC contains first-order "hunger neurons," which express agouti-related peptide (AgRP) and are known to be activated in response to energy deficit (Hahn et al., 1998). These data validated that this approach could be used to reliably detect changes in brain activity in response to energy deficit.

We also identified Fos activation after fasting in a number of other brain regions, including the midbrain, thalamus, and other subregions of the hypothalamus (Table S1). We observed an especially high level of Fos expression in the DRN/ventrolateral periaqueductal gray (vlPAG) region of the brainstem (Figures 1C and 1D). Optical sagittal slices of the brains revealed that this increase in activity was limited to the anterior half of the DRN (Figure 1C). A coronal projection of the sagittal data through the anterior half of the DRN revealed a strong and statistically significant increase in the number of Fos^+ neurons in the interfascicular and dorsal parts of the DRN, as well as in the vlPAG after an overnight fast (Figure 1D). We validated these results using immunohistochemistry (IHC) and found that subsets of neurons in the DRN are indeed activated in fasted mice and also in mice that were re-fed after an overnight fast (Figure S1A). Injections of ghrelin, the levels of which are increased by fasting, also induced significant Fos expression in the DRN (Figure S1B), while water deprivation had no effect (Figure S1C). These results suggested that the DRN is involved in controlling energy homeostasis and raises the question of which cell types within the DRN were activated by changes in energy balance.

We focused on two of the principal neural populations in the DRN: GABAergic neurons that express the vesicular GABA transporter Vgat (*Slc32a1*) and glutamatergic neurons that express the vesicular glutamate transporter VGLUT3 (*Slc17a8*). We crossed Vgat-IRES-Cre or VGLUT3-IRES-Cre mice to Cre-dependent GFPL10 reporter mice, which enabled the selective labeling of DRN^{Vgat} or DRN^{VGLUT3} neurons, respectively. We then evaluated Fos expression in three groups: mice fed ad libitum (fed), mice fasted overnight (fasted), or mice re-fed for 2 hr after an overnight fast (refed). Mice from these groups were then immediately sacrificed after which IHC for Fos was performed. We found a significantly increased number of Fos^+ cells that were Vgat-positive in overnight fasted mice, as compared to fed mice (~51% of Fos^+ neurons in fasted mice versus 19% in fed mice); the number of Fos^+ cells positive for Vgat fell significantly after 2 hr of re-feeding (~33% of Fos^+ cells), but not to basal levels (Figure 1E). In contrast, we found a significantly increased induction of Fos^+ neurons that were VGLUT3-positive in refed mice, as compared to fasted and fed mice (~50% of Fos^+ neurons in refed mice versus ~11% of Fos^+ neurons in both fed and fasted mice). Together, these data suggest that DRN^{Vgat} neurons are activated by fasting, while DRN^{VGLUT3} neurons are activated by re-feeding.

DRN^{Vgat} and DRN^{VGLUT3} Neurons Regulate Food Intake

To initially assess the functional role of the DRN in controlling feeding, we inhibited all neurons by local infusion of selective $GABA_A$ receptor agonist muscimol. Consistent with a previous report (Bendotti et al., 1986), infusion of muscimol into the DRN of mice potently increased food intake (Figure S2A), suggesting that increased GABAergic tone within the DRN induces feeding. We next used optogenetic approaches to test whether direct activation of DRN^{Vgat} neurons was similarly capable of modulating food intake (Figure 2A). We injected Cre-dependent AAV5-EF1a-DIO-ChR2-EYFP into the DRN of Vgat-IRES-Cre mice (Figure 2A, left) and found that these neurons followed spike trains of up to 20 Hz with high fidelity (Figure S2B). We then tested the effect of photostimulating DRN^{Vgat} neurons on food intake in mice fed ad libitum in a 1-hr home cage feeding task, comprised of three 20-min epochs (pre-stimulation, stimulation, post-stimulation). Photoactivation of DRN^{Vgat} neurons with stimulation of 5, 10, and 20 Hz led to a scalable and significant increase in acute food consumption (Figure 2B). A sample trace of control and Vgat:ChR2 mice stimulated at 20 Hz is shown in Figure 2C. Photoactivating DRN^{Vgat} neurons after an overnight fast also led to enhanced re-feeding (Figure S2C). We next tested whether inhibiting these neurons could suppress feeding. We thus injected Cre-dependent AAV5-EF1a-DIO-eArch3.0-EYFP into the DRN of Vgat-IRES-Cre mice (Figure 2A, left). We found that optogenetic photoinhibition of DRN^{Vgat} neurons significantly reduced food intake in fasted mice (Figure 2D). These data together demonstrate that DRN^{Vgat} neurons can bidirectionally control food intake.

We then asked whether these neurons could modulate locomotor activity (Figure 2A, right). To test whether locomotion is altered by DRN^{Vgat} modulation, we performed an open field test (OFT), comprised of three 5-min epochs (pre-stimulation, stimulation, post-stimulation). Optogenetic photoactivation of DRN^{Vgat} neurons at maximal stimulation (20 Hz) had no effect on locomotor activity (Figures 2E and 2F). However, inhibition of these neurons significantly increased movement during the stimulation epoch (Figures 2E and 2G). Neither of these manipulations resulted in any changes in OFT center time, a surrogate measure of anxiety (Figure S2D and data not shown). These data thus demonstrate that inhibiting DRN^{Vgat} neurons can significantly augment locomotor activity. We next evaluated the effect of modulating DRN^{VGLUT3} neurons on food intake and locomotion.

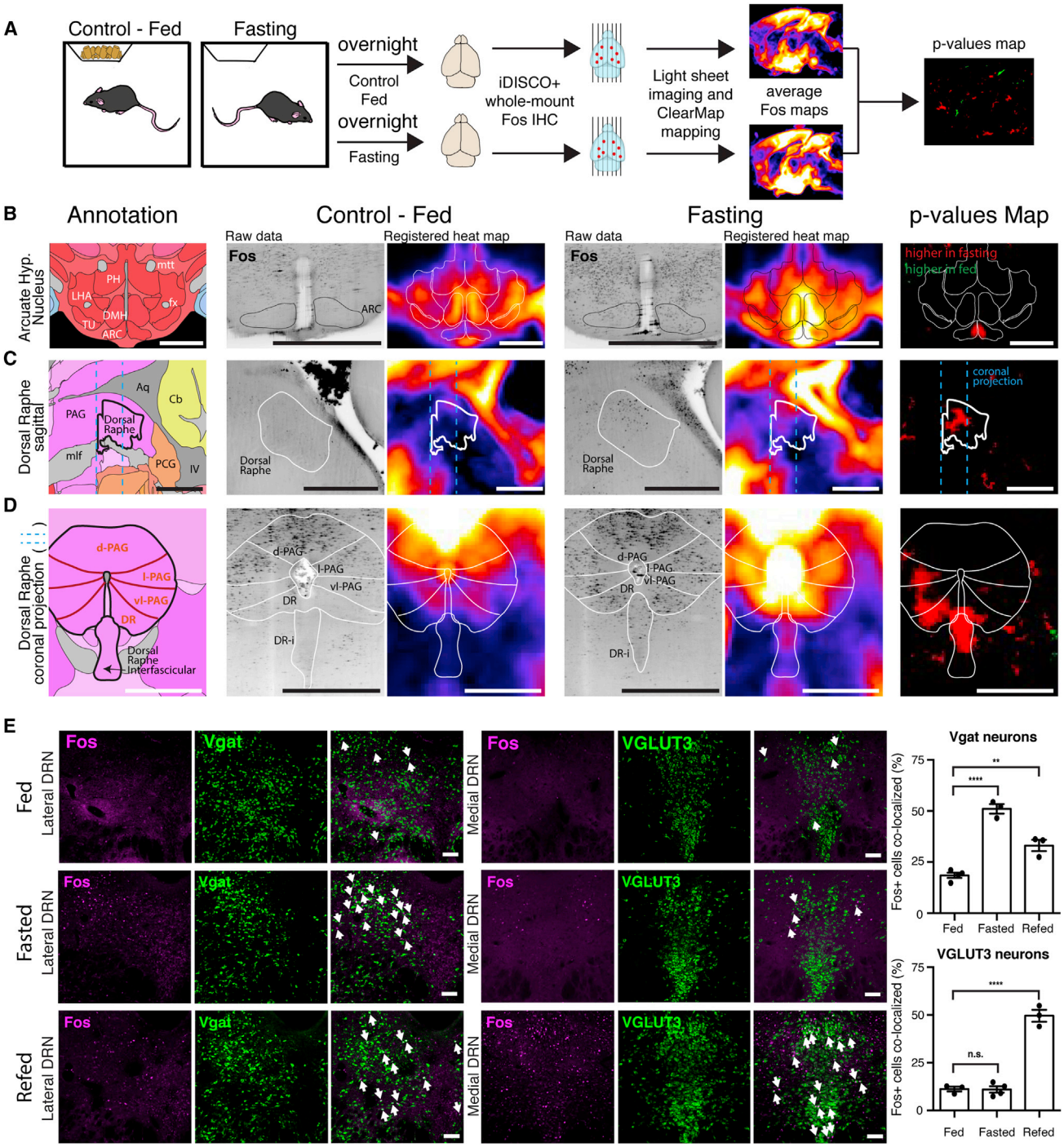

Figure 1. Brain-wide Neuronal Activity in Response to Changes in Metabolic State

(A) Schema for whole-brain activity mapping in fed and fasted mice.

(B–D) Fos mapping results for hypothalamus (B), and DRN from sagittal (C), and compressed coronal (D) views. First column represents the Allen Brain Atlas annotation for hypothalamus (top) and DRN (middle, bottom). Subdivisions of the DRN/PAG were added manually from the Paxinos annotation. Fos raw data, heatmaps, and p values maps are also represented for the fed and fasted states. p values maps demonstrate regions significantly activated in the fasted (red) or fed (green) states. Scale bars, 1 mm.

(E) DRN^{Vgat} neurons are activated in fasted mice, and DRN^{VGLUT3} neurons are activated in re-fed mice. One-way ANOVA comparing fasted and refed to fed mice ($p < 0.0001$ for both DRN^{Vgat} and DRN^{VGLUT3} neurons; n = 3–4 mice per group). White arrows designate double-labeled cells. Scale bars, 100 μm.

**$p < 0.01$, ****$p < 0.0001$. Data are presented as mean ± SEM.

See also Figure S1 and Table S1.

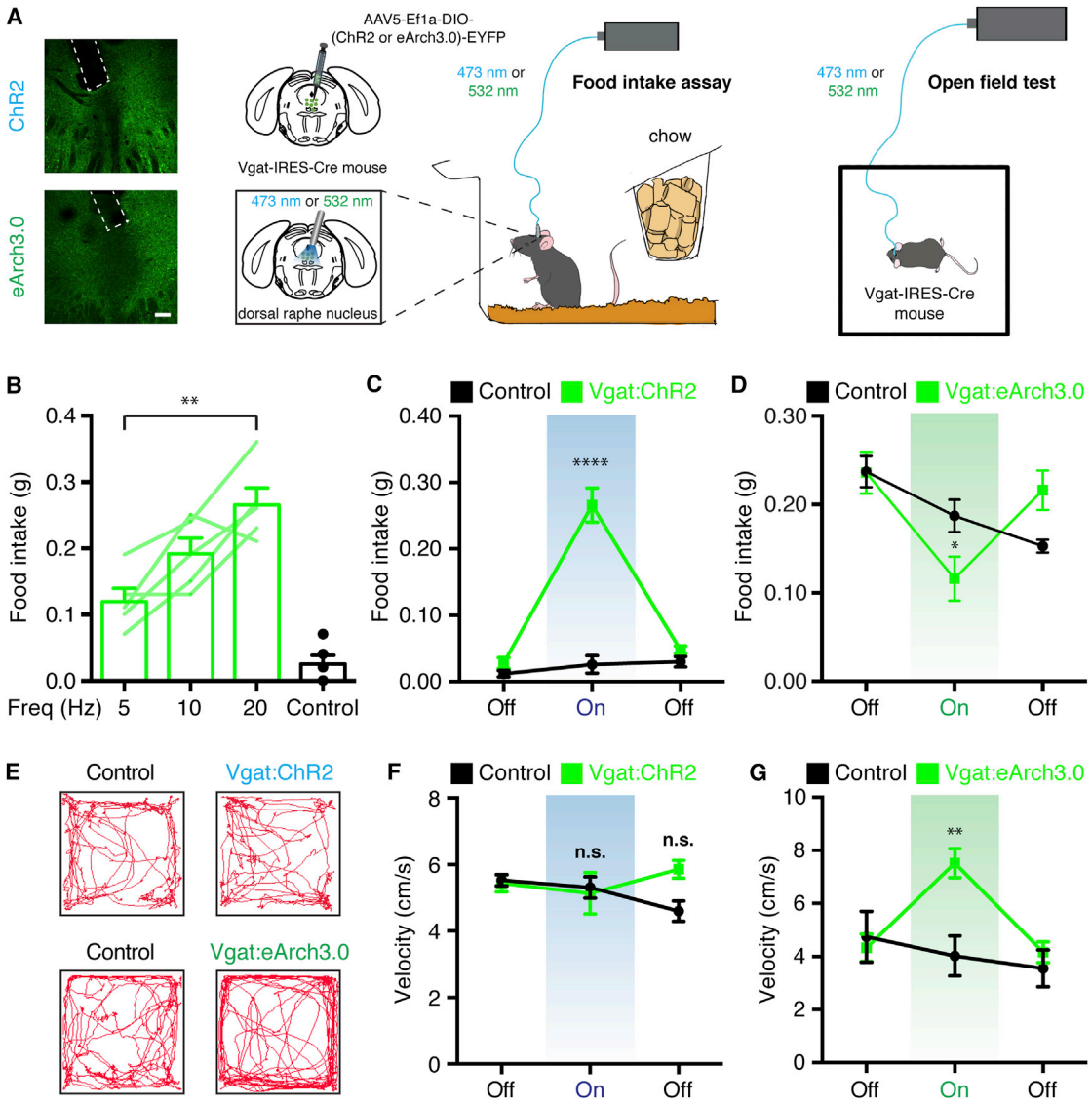

Figure 2. Optogenetic Modulation of DRN^{Vgat} Neurons Bidirectionally Controls Feeding and Increases Locomotion

(A) Representative IHC and fiber optic placement (dashed white lines) for DRN^{Vgat} neurons expressing ChR2-EYFP or eArch3.0-EYFP (left). Schemata for assessing acute food intake (middle) and locomotor activity (right).

(B) Optogenetic photoactivation of DRN^{Vgat} neurons in mice fed ad libitum. Photoactivation of DRN^{Vgat} neurons significantly increases food intake and is scalable. Repeated-measures one-way ANOVA comparing stimulation at 5, 10, and 20 Hz ($p < 0.01$; n = 5 mice per group).

(C and D) Photoactivation (20 Hz) of Vgat:ChR2 mice increases food intake compared to control mice fed ad libitum (C), whereas photoinhibition of Vgat:eArch3.0 mice decreases food intake compared to control mice fasted overnight (D). Two-way ANOVA comparing treated and control groups (n = 5–7 mice per group).

(E) Representative locomotor activity traces for optogenetic activation (top) or inhibition (bottom) of DRN^{Vgat} neurons. Traces taken from stimulation (Laser On) epoch.

(F and G) Optogenetic photoactivation of DRN^{Vgat} neurons does not alter acute locomotor activity (F), while photoinhibition of DRN^{Vgat} neurons significantly increases locomotor activity (G). Two-way ANOVA comparing treated and control mice (n = 5–10 mice per group).

Scale bar, 100 μm. n.s., not significant, *$p < 0.05$, **$p < 0.01$, ****$p < 0.0001$. Data are presented as mean ± SEM. See also Figure S2.

To activate DRN^{VGLUT3} neurons, we injected AAV5-EF1a-DIO-ChR2-EYFP into the DRN of VGLUT3-IRES-Cre mice (Figure 3A, left) and demonstrated that DRN^{VGLUT3} neurons consistently followed spike trains of up to 10 Hz (Figure S3A). We then performed the same 1-hr food intake assay that was used above. We found that photoactivating DRN^{VGLUT3} neurons with stimulation frequencies of 1, 5, and 10 Hz in mice fasted overnight led to an acute and scalable suppression of food intake (Figure 3B). With maximal photostimulation of DRN^{VGLUT3} neurons at 10 Hz, food intake was negligible during stimulation despite the fasted state of the animals (Figure 3C). However, this effect was not observed when the mice were fed ad libitum, due to low basal levels of food intake in sated mice during the testing period (Figure S3B). We then performed optical inhibition studies

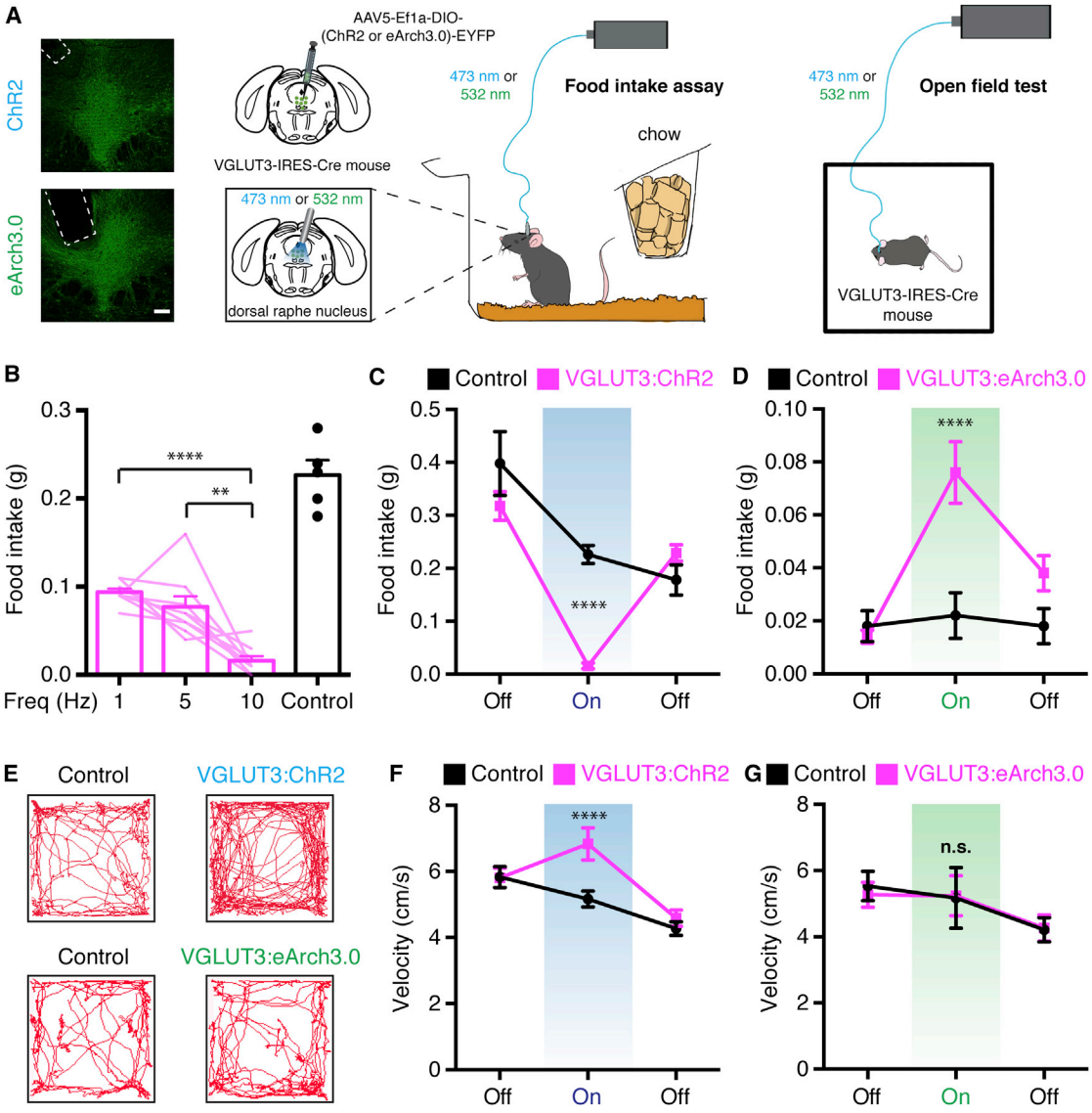

Figure 3. Optogenetic Modulation of DRN^{VGLUT3} Neurons Bidirectionally Controls Feeding and Increases Locomotion

(A) Representative IHC and fiber optic placement (dashed white lines) for DRN^{VGLUT3} neurons expressing ChR2-EYFP or eArch3.0-EYFP. Schemata to assess food intake (middle) or locomotor activity (right).

(B) Photoactivation of DRN^{VGLUT3} neurons in fasted mice significantly suppresses food intake relative to controls in a scalable fashion. Repeated-measures one-way ANOVA comparing mice stimulated at 1, 5, and 10 Hz ($p < 0.001$; n = 5–9 mice per group).

(C and D) Optical activation (10 Hz) of VGLUT3:ChR2 mice suppresses appetite compared to control mice fasted overnight (C). Optical inhibition of VGLUT3:eArch3.0 mice increases feeding compared to control mice fed ad libitum (D). Two-way ANOVA comparing treated and control groups (n = 5–9 mice per group).

(E) Representative locomotor activity traces for optical activation (top) or inhibition (bottom) of DRN^{VGLUT3} neurons. Traces taken from stimulation (Laser On) epoch.

(F and G) Photoactivation of DRN^{VGLUT3} neurons significantly increases locomotor activity (F), whereas photoinhibition of DRN^{VGLUT3} neurons has no effect on locomotion (G). Two-way ANOVA comparing treated and control groups (n = 5–24 mice per group).

Scale bar, 100 μm. n.s., not significant, $^{**}p < 0.01$, $^{****}p < 0.0001$. Data are presented as mean ± SEM. See also Figure S3.

by injecting AAV5-EF1a-DIO-eArch3.0-EYFP into the DRN of VGLUT3-IRES-Cre mice, asking whether inhibiting these neurons could increase feeding (Figure 3A, left). Optical inhibition of DRN^{VGLUT3} neurons led to a significant increase in food intake (Figure 3D), demonstrating that these neurons are also capable of bidirectionally modulating food intake in a reciprocal fashion to that of DRN^{Vgat} neurons.

We also tested whether DRN^{VGLUT3} neuron modulation could induce changes in locomotor activity in the OFT, as described above. Optical activation of DRN^{VGLUT3} neurons at 10 Hz

significantly increased acute locomotor activity (Figures 3E and 3F), while inhibition of DRN^{VGLUT3} neurons had no effect on movement (Figures 3E and 3G). Modulation of these neurons had no measurable effect on OFT center time (Figure S3C and data not shown).

These data together demonstrate that acute manipulation of DRN^{Vgat} and DRN^{VGLUT3} neurons can reciprocally and bidirectionally control feeding and augment locomotor activity.

DRN^{Vgat} and DRN^{VGLUT3} Neurons Modulate Feeding over Prolonged Timescales

We next used designer receptors exclusively activated by designer drugs (DREADDs) to test whether modulating DRN^{Vgat} and DRN^{VGLUT3} neurons could regulate feeding over longer timescales (Sternson and Roth, 2014). DREADDs enable sustained chemogenetic activation or inhibition of neurons using designer ligand clozapine N-oxide (CNO). AAVs encoding either the excitatory DREADD hM3D(Gq) (AAV5-hSyn-DIO-hM3D (Gq)-mCherry) or the inhibitory DREADD hM4D(Gi) (AAV5-hSyn-DIO-hM4D(Gi)-mCherry) were injected into the DRN of Vgat-IRES-Cre or VGLUT3-IRES-Cre mice (Figures 4A and 4B, left). After acclimation to sham injections, CNO was injected intraperitoneally (i.p.) and food intake was measured for 4 hr in the home cage. We found that chemogenetic activation of DRN^{Vgat} neurons significantly increased food intake, while chemogenetic activation of DRN^{VGLUT3} neurons suppressed food intake, thus recapitulating the effects of optical activation over a longer time interval (Figure 4A). Furthermore, in both cases we found that chemogenetic inhibition had the opposite effects, with inhibition of DRN^{Vgat} neurons decreasing food intake and inhibition of DRN^{VGLUT3} neurons increasing food intake (Figure 4B). In control experiments, we found no differences in food intake between control and treated mice after injections of vehicle (Figures S4A and S4B). The aggregate data thus demonstrate that modulation of DRN^{Vgat} and DRN^{VGLUT3} neurons is able to potently and reciprocally control feeding over the course of several hours.

Because DRN^{Vgat} and DRN^{VGLUT3} neurons have opposite effects on feeding, we tested the possibility of crosstalk between these two populations. DRN^{Vgat} neurons are known to make local connections within the DRN (Weissbourd et al., 2014), leading us to hypothesize that they may inhibit DRN^{VGLUT3} neurons. To accomplish this aim, we used ChR2-assisted circuit mapping (CRACM) (Petreanu et al., 2007). We thus injected a mixture of two AAVs, AAV5-EF1a-DIO-mCherry and AAV5-EF1a-'Cre-out'-ChR2-EYFP, into the DRN of VGLUT3-IRES-Cre mice. AAV5-EF1a-DIO-mCherry selectively labels Cre-positive DRN^{VGLUT3} neurons, whereas AAV5-EF1a-'Cre-out'-ChR2-EYFP leads to ChR2-EYFP expression in non-VGLUT3 neurons in the DRN, including DRN^{Vgat} neurons, as Cre expression in the VGLUT3 neurons excises and inactivates expression of ChR2-EYFP (Figure 4C). Slice preparations were made from the DRN of animals receiving the mixed AAV injections, followed by recordings from mCherry-positive DRN^{VGLUT3} neurons during local photostimulation to activate terminals of ChR2-expressing cells. We isolated synaptic currents specifically from local GABAergic (DRN^{Vgat}) neurons by recording after bath addition of kynurenic acid to block out excitatory amino acid currents, which could originate from other local excitatory inputs. We observed light-evoked inhibitory postsynaptic currents (IPSCs) in 9/21 DRN^{VGLUT3} neurons. In the presence of the $GABA_A$ receptor antagonist picrotoxin, IPSCs were blocked in seven of the nine neurons responding to optical stimulation (Figure 4C). These data confirm that DRN^{VGLUT3} neurons can be inhibited by local GABAergic inputs.

Modulation of DRN^{Vgat} and DRN^{VGLUT3} Neurons in Obese Mice

DRN^{VGLUT3} activation and DRN^{Vgat} inhibition decreases food intake and increases locomotor activity, effects which are qualitatively similar to leptin treatment of *ob*/*ob* mice, which are markedly hyperphagic and profoundly hypoactive at baseline (Ribeiro et al., 2011). We first tested whether acute activation of DRN^{VGLUT3} neurons could suppress these abnormalities by crossing VGLUT3-IRES-Cre mice to *ob*/*ob* mice (Zhang et al., 1994) and injecting the DRN with AAV5-EF1a-DIO-ChR2-EYFP. The food intake assay was then performed as previously described (Figure 5A). Photostimulation of DRN^{VGLUT3} neurons at 10 Hz in obese mice led to a significant suppression of feeding (Figure 5B). Acute stimulation of DRN^{VGLUT3} neurons also significantly increased locomotor activity in *ob*/*ob* mice (Figure 5C), with photostimulated mice showing a similar level of activity to wild-type animals (Figure 5D). Activation of DRN^{VGLUT3} neurons thus recapitulates two of the principal effects of leptin treatment on *ob*/*ob* mice.

Chemogenetic inhibition of DRN^{Vgat} neurons also suppressed appetite (Figure 4), suggesting that chronic modulation of these neurons might also reduce food intake and body weight in obese mice. To test this, we crossed Vgat-IRES-Cre mice to *ob*/*ob* mice and followed by injection of AAV5-hSyn-DIO-hM4D(Gi)-mCherry into the DRN (Figure 5A, right). Chronic treatment with designer ligand CNO reduced food intake (Figure 5E) and markedly suppressed the body weight of *ob*/*ob* mice, with the treated animals losing over half of their excess weight (Figure 5F). After removal of CNO treatment, the mice immediately began to regain weight, indicating that persistent inhibition of DRN^{Vgat} neurons is required to sustain weight loss.

Overall, our data show that modulation of neurons in the DRN can reduce food intake in wild-type and obese mice. In principle, similar effects could potentially be elicited by modulating the activity of DRN^{Vgat} and DRN^{VGLUT3} neurons using drugs that engage receptors expressed specifically in these cells. We thus set out to evaluate this possibility by molecularly profiling these neurons.

DRN^{Vgat} and DRN^{VGLUT3} Neurons Are Molecularly Distinct

DRN^{Vgat} and DRN^{VGLUT3} neurons were profiled using viral translating ribosome affinity purification (vTRAP) (Ekstrand et al., 2014; Nectow et al., 2015, 2017). TRAP technology employs a ribosomal subunit protein (RPL10A) fused to EGFP (Heiman et al., 2008), providing a specific epitope for polysome immunoprecipitation (IP). In vTRAP, a Cre-dependent version of this fusion protein (hereafter GFPL10) is expressed from an AAV and yields equivalent results to that of transgenic approaches (Nectow et al., 2017). In the current iteration of vTRAP, we used a novel

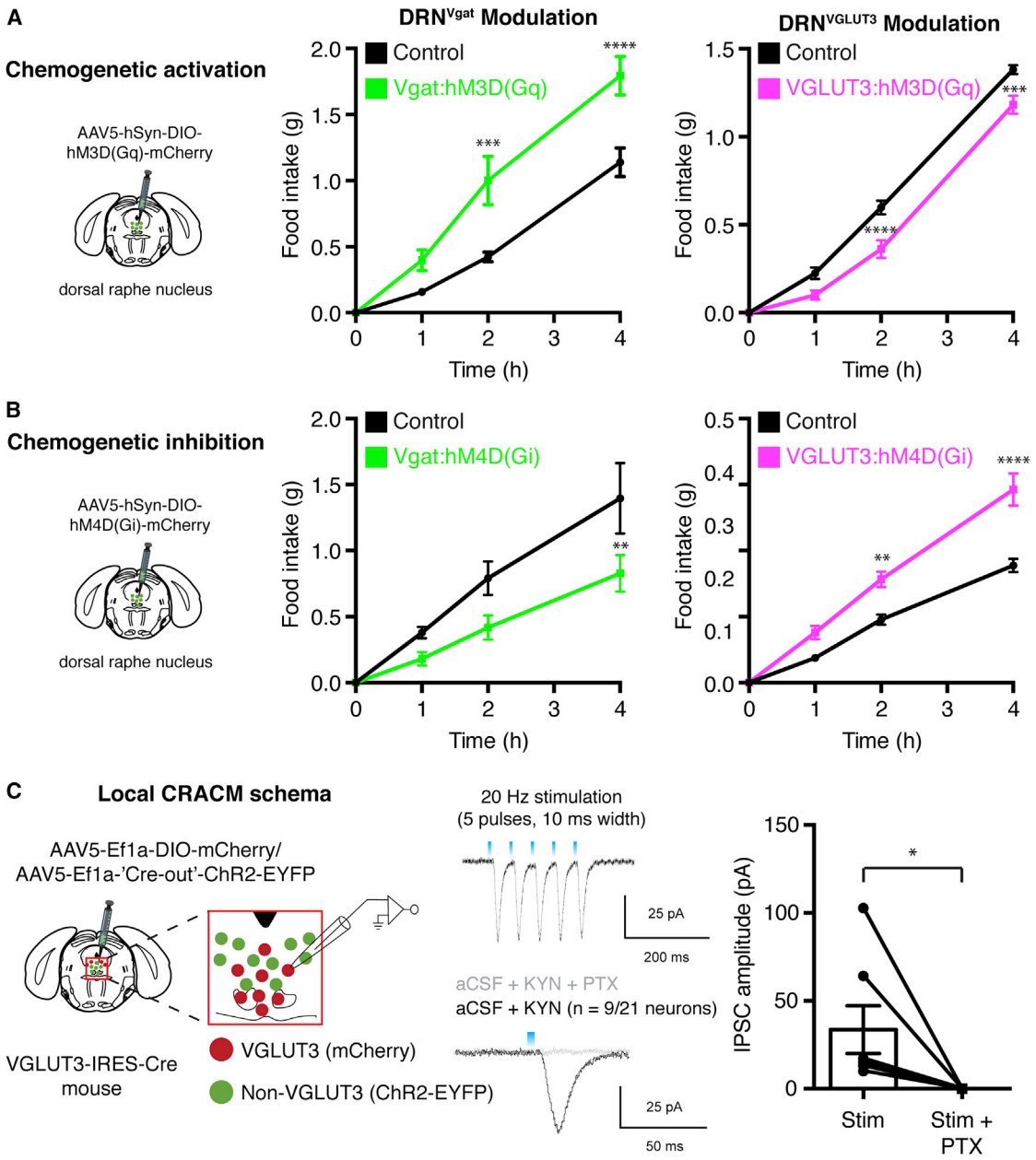

Figure 4. DRN^{Vgat} and DRN^{VGLUT3} Neurons Control Feeding over Hours

(A) Chemogenetic activation of DRN^{Vgat} and DRN^{VGLUT3} neurons. DREADD-induced activation of DRN^{Vgat} neurons significantly increases ($p < 0.01$), whereas activation of DRN^{VGLUT3} neurons suppresses ($p < 0.01$), food intake over the course of 4 hr. Two-way ANOVA comparing treated and control groups (n = 5–6 mice per group).

(B) Chemogenetic inhibition of DRN^{Vgat} and DRN^{VGLUT3} neurons. DREADD-induced inhibition of DRN^{Vgat} neurons significantly suppresses ($p < 0.05$), whereas inhibition of DRN^{VGLUT3} neurons increases ($p < 0.001$), food intake over the course of 4 hr. Two-way ANOVA comparing treated and control groups (n = 4–7 mice per group).

(C) Mapping local inhibitory connections from DRN^{Vgat} neurons onto DRN^{VGLUT3} neurons using CRACM. DRN^{VGLUT3} neurons express mCherry; non-VGLUT3 DRN neurons express ChR2-EYFP. Optical (473 nm) stimulation in the DRN in the presence of KYN elicited IPSCs in 9/21 neurons (middle); 7/9 IPSCs could be blocked by PTX (right).

*$p < 0.05$, **$p < 0.01$, ***$p < 0.001$, ****$p < 0.0001$. Data are presented as mean ± SEM. See also Figure S4.

configuration of lox sites to create a high fidelity "on-off" switch referred to as "Introvert" (Pomeranz et al., 2017) to eliminate Cre-independent expression of GFPL10. This approach is analogous to double-floxed inverted ORF cassettes (DIO/FLEX) (Atasoy et al., 2008). The "Introvert" construct (hereafter AAV5-IV-GFPL10, Figure 6A) contains a GFP sequence in the reverse

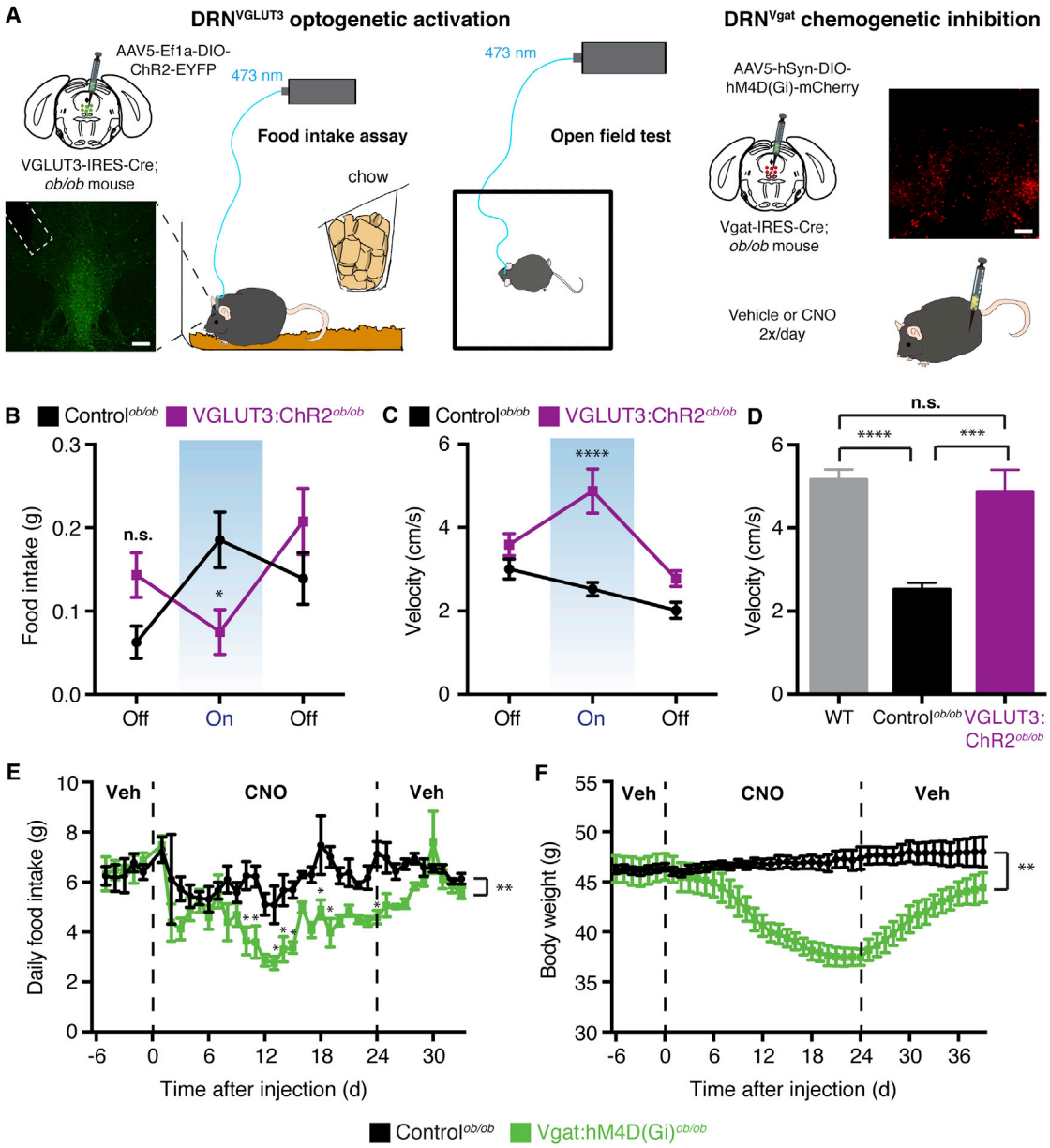

Figure 5. DRN Neural Modulation Resolves Core Features of Obesity

(A) Schemata for optical activation of DRN^{VGLUT3} neurons in the food intake assay (left) and open field test (middle), as well as chronic chemogenetic inhibition of DRN^{Vgat} neurons (right) in obese (*ob/ob*) mice. Representative IHC and fiber optic placement (dashed white lines) for DRN^{VGLUT3} neurons expressing ChR2-EYFP (left), and DRN^{Vgat} neurons expressing hM4D(Gi)-mCherry (right).

(B) Optogenetic photoactivation of DRN^{VGLUT3} neurons in obese mice significantly suppresses food intake relative to controls. Two-way ANOVA comparing treated and control mice (n = 11–12 mice per group).

(C) Photoactivation of DRN^{VGLUT3} neurons in obese mice significantly increases acute locomotor activity (middle). Two-way ANOVA comparing treated and control mice (n = 12–13 mice per group).

(D) DRN^{VGLUT3} photoactivation restores locomotor activity of *ob/ob* mice to wild-type levels. One-way ANOVA comparing treatments ($p < 0.0001$; n = 12–24 mice per group). Data are taken from stimulation epochs in (C) (*ob/ob* and VGLUT3:ChR2$^{ob/ob}$) and Figure 3F (WT).

(E and F) Food intake (E) and body weight (F) of obese mice are significantly reduced after chronic inhibition of DRN^{Vgat} neurons using CNO (2×/day). Two-way ANOVA comparing treated and control mice for food intake ($p < 0.01$) and body weight ($p < 0.01$; n = 5 mice per group). Food intake is significantly different between treated and control mice ($p < 0.05$) where indicated. Body weights of treated mice are significantly different from control mice ($p < 0.05$) days 11-34. Veh, vehicle; CNO, clozapine N-oxide.

Scale bars, 100 μm. *$p < 0.05$, **$p < 0.01$, ***$p < 0.001$, ****$p < 0.0001$. Data are presented as mean ± SEM.

orientation and is flanked by a DIO/FLEX cassette and a split intron, followed by L10 (Figure 6A). We validated this construct in vitro (Figures S5A–S5E) and then generated AAV5-IV-GFPL10.

We injected AAV5-IV-GFPL10 into the DRN of either Vgat-IRES-Cre or VGLUT3-IRES-Cre mice (Figure 6B, left). After waiting 3–4 weeks to allow GFPL10 incorporation into ribosomes, we isolated polysomes from the brainstem by GFP IP (Figure 6B, right) (Heiman et al., 2008). Cell-type-specific isolation of translating mRNAs was confirmed by performing qPCR assays for Vgat (*Slc32a1*) and VGLUT3 (*Slc17a8*), as well as the oligodendrocyte marker gene *Mal* (Schaeren-Wiemers et al., 1995). In these studies, fold-enrichment for a given RNA is calculated as a ratio of the IP RNA abundance divided by the total (input) RNA abundance. As expected, we found that principal marker genes Vgat and VGLUT3 were significantly enriched in the two corresponding populations with 6.6-fold differential enrichment for Vgat (*Slc32a1*) and 38-fold differential enrichment for VGLUT3 (*Slc17a8*) (Figure 6C). As expected, we also found that mRNA for the glial marker gene *Mal* was depleted from both DRN^{Vgat} and DRN^{VGLUT3} IP RNA samples (Figure 6C).

We next performed RNA sequencing (RNA-seq) on the IP and input RNA samples to identify transcripts that were expressed specifically in either DRN^{Vgat} or DRN^{VGLUT3} neurons. We found statistically significant enrichments ($q < 0.05$) of >1.5-fold for 2,390 transcripts in DRN^{Vgat} neurons (Figure 6D, top) and 803 transcripts in DRN^{VGLUT3} neurons (Figure 6D, bottom). By comparing these two datasets, we were able to identify 623 genes that were at least 1.5-fold differentially enriched (DE) between these two populations (Figure 6E), 489 of which were significantly enriched in DRN^{Vgat} neurons and 134 of which were significantly enriched in DRN^{VGLUT3} neurons.

We next validated the specificity of genes for DRN^{Vgat} and DRN^{VGLUT3} neurons, calculating differential expression between the two populations. Differential enrichment for markers isolated from DRN^{Vgat} neurons included Vgat (*Slc32a1*; 7.6-fold DE), GAD67 (*Gad1*; 3.1-fold DE), and GAD65 (*Gad2*; 3.5-fold DE) (Figure 6F). In contrast, we found a 405-fold DE for VGLUT3 (*Slc17a8*) in DRN^{VGLUT3} neurons, while two other glutamate transporters, VGLUT1 (*Slc17a7*) and VGLUT2 (*Slc17a6*), were depleted from both cell types (Figure 6G). Of note, VGLUT3 is co-expressed with serotonin in a subpopulation of DRN neurons (El Mestikawy et al., 2011; Hioki et al., 2010; Okaty et al., 2015). Consistent with this finding, we observed enrichment for serotonin-specific marker genes SERT (*Slc6a4*; 469-fold DE) and tryptophan hydroxylase 2 (*Tph2*; 148-fold DE) (Figure 6H), demonstrating overlap between DRN^{VGLUT3} and DRN serotonin neurons, with limited to no overlap of markers for serotonin and DRN^{Vgat} neurons (Hioki et al., 2010; Weissbourd et al., 2014). Dopamine neurons comprise another subpopulation in the DRN, and as expected, we found an ~4- to 7-fold depletion of the dopaminergic marker genes DAT (*Slc6a3*) and tyrosine hydroxylase (*Th*) from both DRN^{Vgat} and DRN^{VGLUT3} neurons (Figure 6I).

Cell-Type-Specific Pharmacology within the DRN Regulates Food Intake

The analysis of gene expression in DRN^{Vgat} and DRN^{VGLUT3} neurons revealed 27 RNAs encoding transmembrane receptors that were differentially enriched between the two cell types (Figure 7A), 19 of which were significantly enriched in DRN^{Vgat} neurons ($q < 0.05$), with 8 significantly enriched in DRN^{VGLUT3} neurons ($q < 0.05$). Ligands for several of these receptors are available, including the inhibitory serotonin autoreceptor 5-HT_{1A} (*Htr1a*; 4.6-fold DE, $q < 0.05$ in DRN^{VGLUT3} neurons), the neuropeptide Y receptor Y2 (*Npy2r*; 10.6-fold DE, $q < 0.05$ in DRN^{VGLUT3} neurons), and the melanocortin 4 receptor (*Mc4r*; 11.6-fold DE, $q < 0.05$ in DRN^{Vgat} neurons) (Figure 7A). We confirmed cell-specific expression of each of these receptors using double fluorescence in situ hybridization (FISH) against either Vgat (*Slc32a1*) or VGLUT3 (*Slc17a8*), in tandem with each of these receptors (*Htr1a*, *Npy2r*, or *Mc4r*) (Figure 7B). These data establish expression of each of these receptors in DRN^{Vgat} or DRN^{VGLUT3} neurons.

We next performed slice electrophysiology to test whether ligands for these receptors were able to modulate neural activity (Figure S6A). DRN^{VGLUT3} and DRN^{Vgat} neurons were labeled by respectively crossing VGLUT3-IRES-Cre or Vgat-IRES-Cre mice to Cre-dependent GFPL10 reporter mice. Bath application of selective 5-HT_{1A} agonist 8-OH-DPAT resulted in a significant inhibition of 6/12 DRN^{VGLUT3} neurons (Figures 7C and S6B), consistent with the finding that 5-HT_{1A} is an inhibitory serotonergic autoreceptor (Richardson-Jones et al., 2010). We next tested the effect of peptide $YY_{3–36}$ ($PYY_{3–36}$), a neuropeptide Y receptor Y2 (NPY_2R) agonist. Bath application significantly activated 5/8 DRN^{VGLUT3} neurons tested (Figures 7D and S6C). We also found that the melanocortin 4 receptor (MC_4R) is preferentially enriched in DRN^{Vgat} neurons and tested the effect of α-melanocyte stimulating hormone (α-MSH), a ligand for MC_4R (Figure 7A) (Balthasar et al., 2005). Bath application of α-MSH led to a significant inhibition of 9/22 DRN^{Vgat} neurons tested (Figures 7E and S6D). This effect is unlikely to be mediated through the melanocortin 3 receptor (MC_3R), as this receptor is not enriched in either DRN^{Vgat} or DRN^{VGLUT3} neurons (Figure S6H). We also showed that the observed effects of each ligand on DRN^{Vgat} or DRN^{VGLUT3} neurons were direct by repeating the above studies under synaptic blockade using kynurenic acid and picrotoxin (Figures S6E–S6G).

We then tested whether the effect of these ligands on DRN^{Vgat} and DRN^{VGLUT3} neural activity was correlated with effects on feeding behavior. Each of these ligands was infused locally into the DRN of wild-type mice and food intake was measured (Figure S6A). Infusion of 8-OH-DPAT, which inhibits DRN^{VGLUT3} neurons, led to a potent and significant increase in food intake (Figure 7F). We next tested the effect of agonizing NPY_2R. Because PYY_{3-36} activates DRN^{VGLUT3} neurons, we hypothesized that this would lead to a suppression of feeding. As predicted, infusion of PYY_{3-36} significantly reduced food intake (Figure 7G). Critically, these effects are consistent with that of optogenetically and chemogenetically modulating DRN^{VGLUT3} neurons (see Figures 3 and 4). Of note, the data using molecular profiling revealed that NPY_2R is the only NPY receptor significantly enriched within DRN^{VGLUT3} neurons, and we thus predicted that NPY would have a similar effect on feeding (Figure S6I). Consistent with this hypothesis, we found that NPY also activates DRN^{VGLUT3}

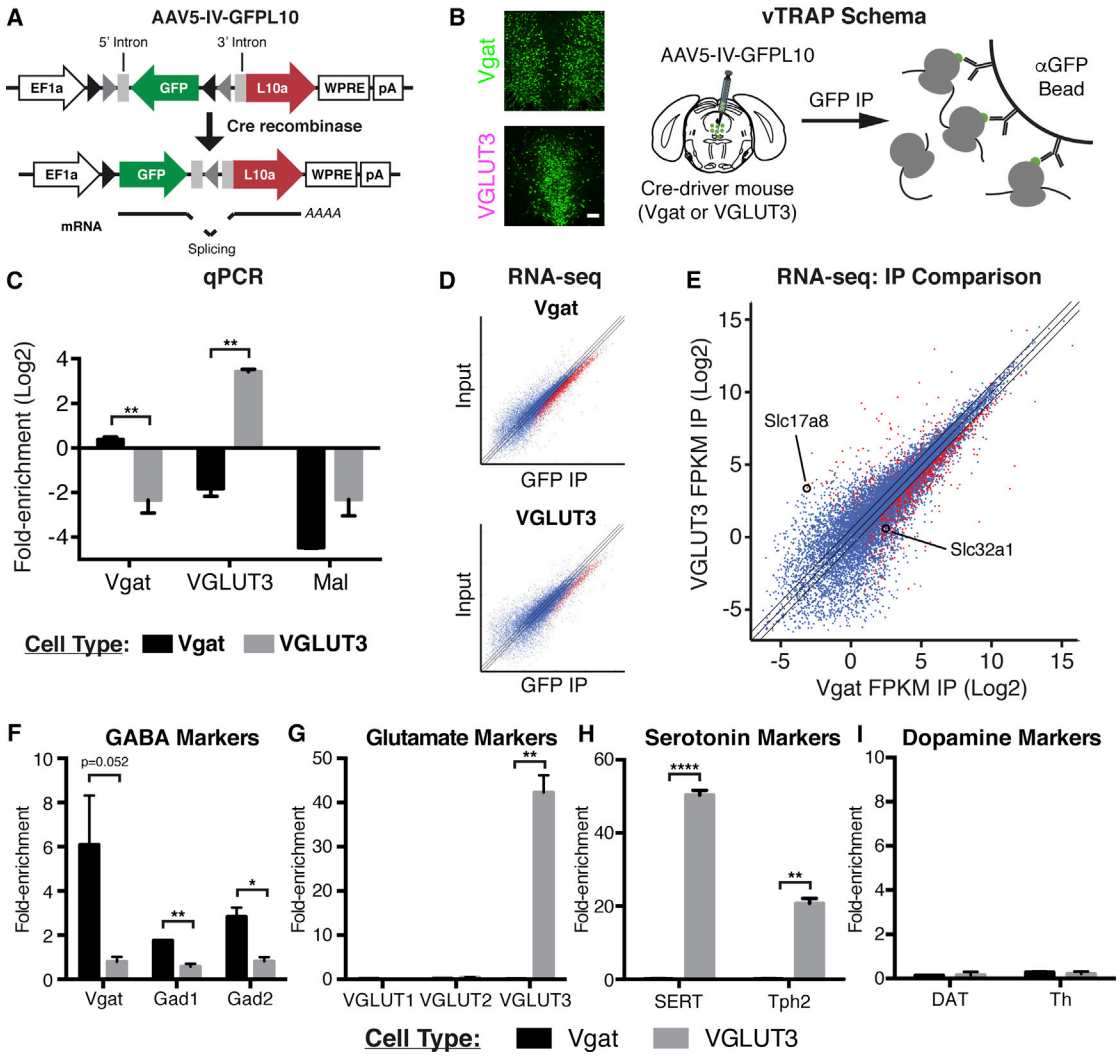

Figure 6. DRN^{Vgat} and DRN^{VGLUT3} Neurons Are Molecularly Distinct

(A) Design of AAV5-IV-GFPL10 (top). In the presence of Cre, GFP is reverted to the forward orientation with a lox site flanked by a split intron (middle). After splicing, mature transcript (bottom) is translated into the GFPL10 fusion protein.

(B) Schema and IHC for vTRAP studies. AAV5-IV-GFPL10 is injected into the DRN of either Vgat-IRES-Cre or VGLUT3-IRES-Cre mice, followed by a GFP IP.

(C) qPCR for cell-type-specific, immunoprecipitated mRNAs. Genes: Vgat (*Slc32a1*), VGLUT3 (*Slc17a8*), and Mal (*Mal*). Unpaired t test comparing Vgat and VGLUT3.

(D) RNA-seq scatterplots for DRN^{Vgat} (top) and DRN^{VGLUT3} (bottom) neurons with normalized expression (fragments per kilobase million [FPKM]). Significantly enriched genes ($q < 0.05$) are displayed in red, and all other genes are displayed in blue. Black lines display unity and 1.5-fold change in enrichment.

(E) Comparison of IP RNA from DRN^{Vgat} and DRN^{VGLUT3} expression data (Log2) from (D). Red genes are significantly enriched ($q < 0.05$ in IP/input comparison and >1.5-fold differentially enriched between Vgat and VGLUT3 neurons); all other genes are displayed in blue. Black lines display unity and 1.5-fold changes in enrichment.

(F–I) Differential enrichments from RNA-seq for marker genes specific to GABAergic (F), glutamatergic (G), serotonergic (H), and dopaminergic (I) neurons. Unpaired t test comparing Vgat and VGLUT3.

Scale bar, 100 μm. *$p < 0.05$, **$p < 0.01$, ****$p < 0.0001$. Data are presented as mean ± SEM. qPCR data are normalized to Rpl23. Enrichment is defined as IP/input. See also Figure S5.

neurons (Figures S6J and S6K) and suppresses food intake (Figure S6L). Of note, this anorexigenic effect of locally administering NPY in the DRN is opposite to the effect of intracerebroventricular infusion of NPY, which increases food intake (Clark et al., 1984).

Finally, we tested the effect of α-MSH, which inhibited DRN^{Vgat} neurons in the slice preparation. Infusion of α-MSH locally within the DRN resulted in a robust suppression of food intake (Figure 7H). These findings are consistent with the effect of optically and chemogenetically inhibiting DRN^{Vgat} neurons (Figures 2 and 4). In aggregate, these data show that pharmacologic modulation of DRN^{Vgat} and DRN^{VGLUT3} neurons can recapitulate the effects of chemogenetic and optogenetic modulation.

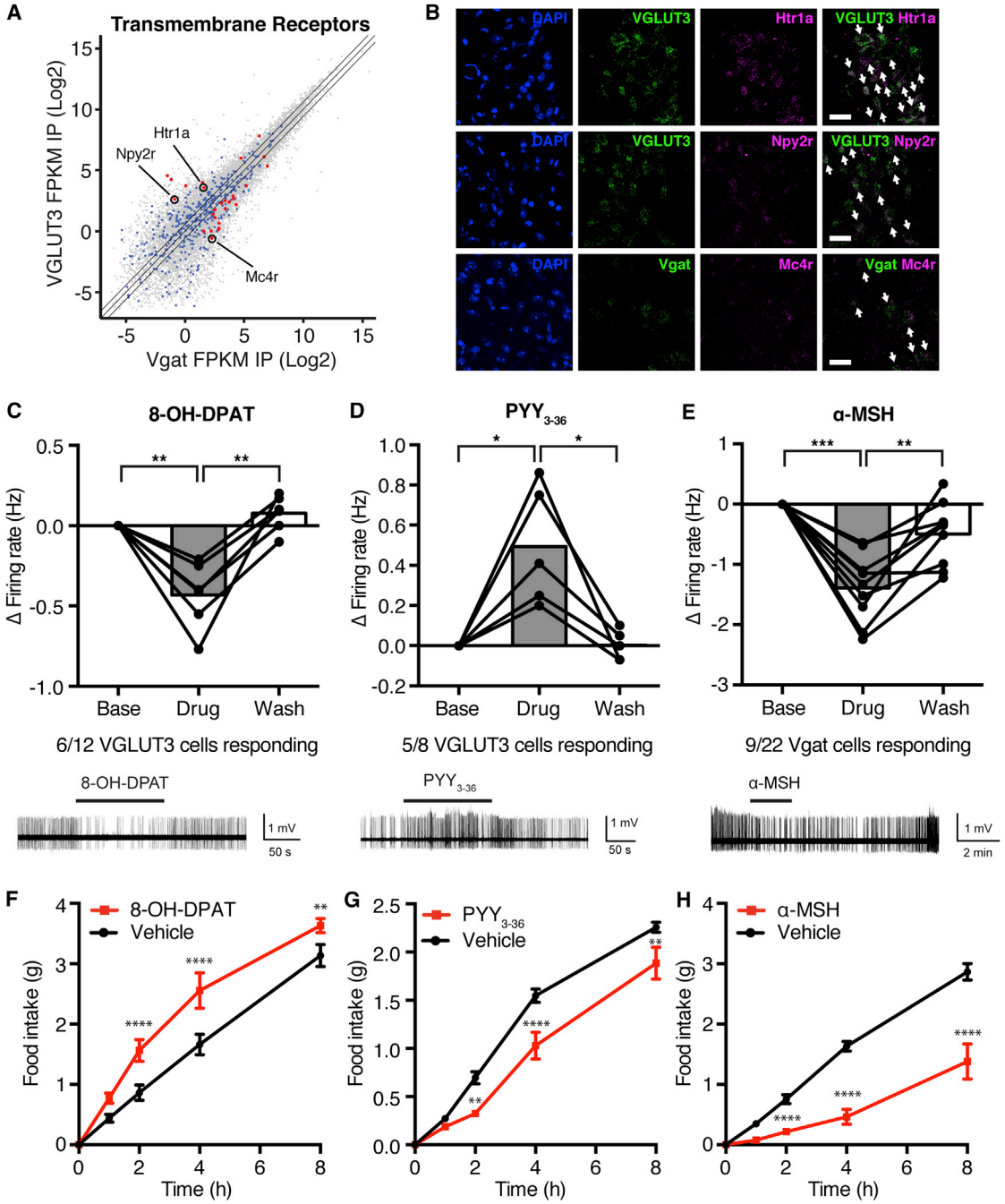

Figure 7. Cell-Type-Specific Receptor Targeting Bidirectionally Modulates Feeding

(A) Scatterplot (Log2) displaying differentially expressed transmembrane receptor genes. Red genes, annotated as transmembrane receptors, 1.5-fold differentially expressed between DRN^{Vgat} and DRN^{VGLUT3} neurons, and significantly enriched in IP/input comparison ($q < 0.05$); blue genes, non-significant annotated transmembrane receptors; gray genes, all other genes.

(B) Colocalization between cell-type-specific marker genes (Vgat or VGLUT3) and receptors (Mc4r, Htr1a, or Npy2r). White arrows designate double-labeled cells.

(C) DRN^{VGLUT3} neurons are inhibited by selective 5-HT_{1A} agonist 8-OH-DPAT (1 μM). 6/12 neurons responded from n = 6 mice. One-way repeated-measures (RM)-ANOVA (treatment: $p < 0.01$). Representative voltage traces of a DRN^{VGLUT3} neuron inhibited by 8-OH-DPAT.

(D) DRN^{VGLUT3} neurons are activated by the selective Neuropeptide Y receptor Y2 agonist $PYY_{3–36}$ (1 μM). 5/8 neurons responded from n = 6 mice. One-way RM-ANOVA (treatment: $p < 0.01$). Representative voltage traces of a DRN^{VGLUT3} neuron activated by $PYY_{3–36}$.

(E) DRN^{Vgat} neurons are inhibited by MC_4R agonist α-MSH (250 nM). 9/22 neurons responded from n = 6 mice. One-way RM-ANOVA (treatment: $p < 0.0001$). Representative voltage traces of a DRN^{Vgat} neuron inhibited by α-MSH.

(legend continued on next page)

DISCUSSION

Feeding behavior is controlled by a distributed network, comprised of many populations in the hypothalamus, brainstem, and limbic system. In the hypothalamus, ARC^{AgRP}, ARC^{POMC}, LH^{Vgat}, and LH^{MCH} neurons, as well as several other populations, have been shown to control feeding and a number of related behaviors (Aponte et al., 2011; Domingos et al., 2013; Jennings et al., 2015). Specific cell populations within the PBN (Carter et al., 2013) and the amygdala/extended amygdala (Cai et al., 2014; Jennings et al., 2013) have also been shown to regulate feeding, and these studies have revealed interconnectivity between a number of these loci. In the current work, we used an unbiased approach to map sites of neural activation and found that subsets of neurons in the DRN are activated in response to fasting and re-feeding, as well to related hormonal cues. These studies led us to hypothesize that the DRN might also regulate feeding, which was consistent with several previous lines of evidence showing that pharmacological manipulation of the DRN can drive food intake (Bendotti et al., 1986; Currie et al., 1994; Fletcher and Davies, 1990), the DRN projects to many regions known to control feeding (Vertes, 1991; Vertes and Kocsis, 1994), and subsets of DRN neurons are activated by feeding (Fornal et al., 1996; Veasey et al., 1997).

In the current study, we focused on DRN^{Vgat} and DRN^{VGLUT3} neurons, finding that they can exert cell-type-specific effects on food intake. We demonstrated that both DRN^{Vgat} and DRN^{VGLUT3} neurons are directly regulated by changes in energy balance (Figure 1) and potently control feeding (Figures 2 and 3). We also found that DRN^{Vgat} neurons inhibit DRN^{VGLUT3} neurons, suggesting a potential local circuit mechanism through which DRN^{Vgat} neurons drive feeding (Figure 4). However, the inputs and outputs of these neurons have not been completely characterized, and further studies will be necessary to determine which sites of projection mediate the observed effects of DRN^{Vgat} and DRN^{VGLUT3} neurons on feeding.

We also found that modulating the activity of DRN^{Vgat} and DRN^{VGLUT3} neurons was able to significantly ameliorate the phenotype of leptin-deficient *ob/ob* mice (Figure 5), suggesting that the effects of modulating DRN activity are independent of leptin action. In general, obese individuals have high endogenous leptin levels and show a diminished response to its exogenous application. The site(s) of leptin resistance in the general population have not been fully characterized and is likely to be heterogeneous (Friedman and Halaas, 1998). One strategy to treat obesity would thus be to identify neurons downstream of the block in leptin action and modulate their activity to control energy balance. The finding that chronically inhibiting DRN^{Vgat} neurons can reduce body weight in obese mice lacking leptin suggests that this might be a feasible approach.

We then evaluated potential pharmacological strategies by using molecular profiling, which enabled us to identify druggable targets in both DRN^{Vgat} and DRN^{VGLUT3} neurons (Figures 6 and 7). We used vTRAP (Nectow et al., 2017) to identify transmembrane receptors that were enriched in these neurons. In each case, the effect of ligands on the firing rate of cells expressing each receptor was associated with the predicted response on feeding. However, while these studies represent a proof of principle that pharmacologically controlling the activity of DRN^{Vgat} and DRN^{VGLUT3} neurons can alter food intake, the molecules we tested are not likely to be drug candidates, as their receptors are expressed in many other brain regions, often with disparate functions. Thus, further mining of druggable targets in these populations may potentially provide a therapeutic approach for controlling energy balance.

In summary, we identify the DRN as an important brainstem node in the expanded neural circuitry controlling food intake. This work suggests a potential strategy for the pharmacologic control of food intake and body weight, as well as the treatment of obesity.

STAR★METHODS

Detailed methods are provided in the online version of this paper and include the following:

- KEY RESOURCES TABLE
- CONTACT FOR REAGENT AND RESOURCE SHARING
- EXPERIMENTAL MODEL AND SUBJECT DETAILS
- METHOD DETAILS
  - Viral Vectors
  - Construction of pAAV-IV-GFPL10
  - Stereotaxic Surgery
  - Cell Culture
  - Molecular Profiling
  - RNA-seq
  - Slice Electrophysiology
  - In Vivo Photostimulation
  - Food Intake Assay for Optogenetic Studies
  - Food Intake Assay for Chemogenetic Studies
  - Food Intake Assay for Pharmacology Studies
  - Open Field Test for Optogenetic Studies
  - iDISCO+ Brain Clearing
- QUANTIFICATION AND STATISTICAL ANALYSIS
- DATA AND SOFTWARE AVAILABILITY
  - Data Resources

SUPPLEMENTAL INFORMATION

Supplemental Information includes six figures and one table and can be found with this article online at http://dx.doi.org/10.1016/j.cell.2017.06.045.

An audio PaperClip is available at http://dx.doi.org/10.1016/j.cell.2017.06.045#mmc2.

(F) 8-OH-DPAT (0.5 μl, 6.4 nmol/μL) delivered into the DRN significantly increases food intake relative to vehicle. Two-way RM-ANOVA ($p < 0.001$; n = 9 mice). (G) PYY_{3-36} (0.5 μl, 200 nmol/μL) delivered into the DRN significantly suppresses food intake relative to vehicle. Two-way RM-ANOVA ($p < 0.01$; n = 8 mice). (H) α-MSH (0.5 μl, 1.2 nmol/μL) delivered into the DRN significantly suppresses food intake relative to vehicle. Two-way RM-ANOVA ($p < 0.001$; n = 9 mice). Scale bars, 25 μm. *$p < 0.05$, **$p < 0.01$, ***$p < 0.001$, ****$p < 0.0001$. Data are presented as mean ± SEM. See also Figure S6.

AUTHOR CONTRIBUTIONS

A.R.N. conceived the study and developed the research program. A.R.N. and J.M.F. designed the study. A.R.N. performed molecular profiling experiments. A.R.N., M.S., B.C.F., and E.A. performed behavioral experiments. H.X. performed slice electrophysiology studies. M.H.H. designed slice electrophysiology studies. M.S., N.R., A.R.N., and M.T.-L. performed iDISCO+ studies. A.R.N., Y.L., and S.M. analyzed RNA-seq data. B.P. assisted with histology. A.R.N., M.S., H.Z., N.R., Y.L., S.M., M.-H.H., and J.M.F. analyzed data. A.R.N. and J.M.F. wrote the manuscript with input from all authors.

ACKNOWLEDGMENTS

We thank Mats Ekstrand for help designing pAAV-IV-GFPL10, Brad Lowell, Linh Vong, and Dong Kong for contributing VGLUT3-IRES-Cre and Vgat-IRES-Cre mice, Chitra Kumar and Varun Bhave for help with chemogenetic studies, Karl Deisseroth for contributing pAAV-EF1a-DIO-ChR2-mCherry, used in the creation of pAAV-IV-GFPL10, Todd Anthony and David Anderson for contributing the virus AAV5-EF1a-'Cre-out'-ChR2-EYFP, Masago Ishikawa and Paul Kenny for help with electrophysiology, Ilana Witten and Eric Nestler for helpful discussions, and The Rockefeller University Genomics and Bio-Imaging Resource Centers. This work is supported by funding from The JPB foundation (CEN 5402133; J.M.F.). A.R.N. acknowledges support from the David Rockefeller Fellowship, the Brain and Behavior Research Foundation NARSAD Young Investigator Award, the Princeton Neuroscience Institute's CV Starr Fellowship and Innovation Award, and The Rockefeller University's Shapiro-Silverberg Fund (CEN5301493). H.Z is supported by the National Natural Science Foundation of China (81200862). M.H.H. acknowledges support from the NIMH (R01MH092306), NIAA, and the Brain and Behavior Research Foundation NARSAD Independent Investigator Award (21464).

Received: November 2, 2016
Revised: May 30, 2017
Accepted: June 28, 2017
Published: July 27, 2017

REFERENCES

Aponte, Y., Atasoy, D., and Sternson, S.M. (2011). AGRP neurons are sufficient to orchestrate feeding behavior rapidly and without training. Nat. Neurosci. *14*, 351–355.

Atasoy, D., Aponte, Y., Su, H.H., and Sternson, S.M. (2008). A FLEX switch targets Channelrhodopsin-2 to multiple cell types for imaging and long-range circuit mapping. J. Neurosci. *28*, 7025–7030.

Balthasar, N., Dalgaard, L.T., Lee, C.E., Yu, J., Funahashi, H., Williams, T., Ferreira, M., Tang, V., McGovern, R.A., Kenny, C.D., et al. (2005). Divergence of melanocortin pathways in the control of food intake and energy expenditure. Cell *123*, 493–505.

Bendotti, C., Berettera, C., Invernizzi, R., and Samanin, R. (1986). Selective involvement of dopamine in the nucleus accumbens in the feeding response elicited by muscimol injection in the nucleus raphe dorsalis of sated rats. Pharmacol. Biochem. Behav. *24*, 1189–1193.

Cai, H., Haubensak, W., Anthony, T.E., and Anderson, D.J. (2014). Central amygdala PKC-δ(+) neurons mediate the influence of multiple anorexigenic signals. Nat. Neurosci. *17*, 1240–1248.

Carlini, V.P., Varas, M.M., Cragnolini, A.B., Schiöth, H.B., Scimonelli, T.N., and de Barioglio, S.R. (2004). Differential role of the hippocampus, amygdala, and dorsal raphe nucleus in regulating feeding, memory, and anxiety-like behavioral responses to ghrelin. Biochem. Biophys. Res. Commun. *313*, 635–641.

Carter, M.E., Soden, M.E., Zweifel, L.S., and Palmiter, R.D. (2013). Genetic identification of a neural circuit that suppresses appetite. Nature *503*, 111–114.

Challis, C., Boulden, J., Veerakumar, A., Espallergues, J., Vassoler, F.M., Pierce, R.C., Beck, S.G., and Berton, O. (2013). Raphe GABAergic neurons mediate the acquisition of avoidance after social defeat. J. Neurosci. *33*, 13978–13988.

Clark, J.T., Kalra, P.S., Crowley, W.R., and Kalra, S.P. (1984). Neuropeptide Y and human pancreatic polypeptide stimulate feeding behavior in rats. Endocrinology *115*, 427–429.

Currie, P.J., Fletcher, P.J., and Coscina, D.V. (1994). Administration of 8-OH-DPAT into the midbrain raphe nuclei: effects on medial hypothalamic NE-induced feeding. Am. J. Physiol. *266*, R1645–R1651.

Domingos, A.I., Vaynshteyn, J., Sordillo, A., and Friedman, J.M. (2013). The reward value of sucrose in leptin-deficient obese mice. Mol. Metab. *3*, 73–80.

Ekstrand, M.I., Nectow, A.R., Knight, Z.A., Latcha, K.N., Pomeranz, L.E., and Friedman, J.M. (2014). Molecular profiling of neurons based on connectivity. Cell *157*, 1230–1242.

El Mestikawy, S., Wallén-Mackenzie, A., Fortin, G.M., Descarries, L., and Trudeau, L.E. (2011). From glutamate co-release to vesicular synergy: vesicular glutamate transporters. Nat. Rev. Neurosci. *12*, 204–216.

Fletcher, P.J., and Davies, M. (1990). Dorsal raphe microinjection of 5-HT and indirect 5-HT agonists induces feeding in rats. Eur. J. Pharmacol. *184*, 265–271.

Fornal, C.A., Metzler, C.W., Marrosu, F., Ribiero-do-Valle, L.E., and Jacobs, B.L. (1996). A subgroup of dorsal raphe serotonergic neurons in the cat is strongly activated during oral-buccal movements. Brain Res. *716*, 123–133.

Friedman, J.M., and Halaas, J.L. (1998). Leptin and the regulation of body weight in mammals. Nature *395*, 763–770.

Friedman, A.K., Walsh, J.J., Juarez, B., Ku, S.M., Chaudhury, D., Wang, J., Li, X., Dietz, D.M., Pan, N., Vialou, V.F., et al. (2014). Enhancing depression mechanisms in midbrain dopamine neurons achieves homeostatic resilience. Science *344*, 313–319.

Garfield, A.S., Li, C., Madara, J.C., Shah, B.P., Webber, E., Steger, J.S., Campbell, J.N., Gavrilova, O., Lee, C.E., Olson, D.P., et al. (2015). A neural basis for melanocortin-4 receptor-regulated appetite. Nat. Neurosci. *18*, 863–871.

Hahn, T.M., Breininger, J.F., Baskin, D.G., and Schwartz, M.W. (1998). Coexpression of Agrp and NPY in fasting-activated hypothalamic neurons. Nat. Neurosci. *1*, 271–272.

Han, M.H., Bolaños, C.A., Green, T.A., Olson, V.G., Neve, R.L., Liu, R.J., Aghajanian, G.K., and Nestler, E.J. (2006). Role of cAMP response element-binding protein in the rat locus ceruleus: regulation of neuronal activity and opiate withdrawal behaviors. J. Neurosci. *26*, 4624–4629.

Heiman, M., Schaefer, A., Gong, S., Peterson, J.D., Day, M., Ramsey, K.E., Suárez-Fariñas, M., Schwarz, C., Stephan, D.A., Surmeier, D.J., et al. (2008). A translational profiling approach for the molecular characterization of CNS cell types. Cell *135*, 738–748.

Hioki, H., Nakamura, H., Ma, Y.F., Konno, M., Hayakawa, T., Nakamura, K.C., Fujiyama, F., and Kaneko, T. (2010). Vesicular glutamate transporter 3-expressing nonserotonergic projection neurons constitute a subregion in the rat midbrain raphe nuclei. J. Comp. Neurol. *518*, 668–686.

Jennings, J.H., Rizzi, G., Stamatakis, A.M., Ung, R.L., and Stuber, G.D. (2013). The inhibitory circuit architecture of the lateral hypothalamus orchestrates feeding. Science *341*, 1517–1521.

Jennings, J.H., Ung, R.L., Resendez, S.L., Stamatakis, A.M., Taylor, J.G., Huang, J., Veleta, K., Kantak, P.A., Aita, M., Shilling-Scrivo, K., et al. (2015). Visualizing hypothalamic network dynamics for appetitive and consummatory behaviors. Cell *160*, 516–527.

Krashes, M.J., Shah, B.P., Madara, J.C., Olson, D.P., Strochlic, D.E., Garfield, A.S., Vong, L., Pei, H., Watabe-Uchida, M., Uchida, N., et al. (2014). An excitatory paraventricular nucleus to AgRP neuron circuit that drives hunger. Nature *507*, 238–242.

Larsen, P.J., Hay-Schmidt, A., Vrang, N., and Mikkelsen, J.D. (1996). Origin of projections from the midbrain raphe nuclei to the hypothalamic paraventricular nucleus in the rat: a combined retrograde and anterograde tracing study. Neuroscience *70*, 963–988.

Li, C., Sugam, J.A., Lowery-Gionta, E.G., McElligott, Z.A., McCall, N.M., Lopez, A.J., McKlveen, J.M., Pleil, K.E., and Kash, T.L. (2016). Mu opioid receptor

modulation of dopamine neurons in the periaqueductal gray/dorsal raphe: a role in regulation of pain. Neuropsychopharmacology *41*, 2122–2132.

Liu, Z., Zhou, J., Li, Y., Hu, F., Lu, Y., Ma, M., Feng, Q., Zhang, J.E., Wang, D., Zeng, J., et al. (2014). Dorsal raphe neurons signal reward through 5-HT and glutamate. Neuron *81*, 1360–1374.

Lou, S., Duan, B., Vong, L., Lowell, B.B., and Ma, Q. (2013). Runx1 controls terminal morphology and mechanosensitivity of VGLUT3-expressing C-mechanoreceptors. J Neurosci. *33*, 870–882.

Matthews, G.A., Nieh, E.H., Vander Weele, C.M., Halbert, S.A., Pradhan, R.V., Yosafat, A.S., Glober, G.F., Izadmehr, E.M., Thomas, R.E., Lacy, G.D., et al. (2016). Dorsal raphe dopamine neurons represent the experience of social isolation. Cell *164*, 617–631.

McDevitt, R.A., Tiran-Cappello, A., Shen, H., Balderas, I., Britt, J.P., Marino, R.A., Chung, S.L., Richie, C.T., Harvey, B.K., and Bonci, A. (2014). Serotonergic versus nonserotonergic dorsal raphe projection neurons: differential participation in reward circuitry. Cell Rep. *8*, 1857–1869.

Nectow, A.R., Ekstrand, M.I., and Friedman, J.M. (2015). Molecular characterization of neuronal cell types based on patterns of projection with Retro-TRAP. Nat. Protoc. *10*, 1319–1327.

Nectow, A.R., Moya, M.V., Ekstrand, M.I., Mousa, A., McGuire, K.L., Sferrazza, C.E., Field, B.C., Rabinowitz, G.S., Sawicka, K., Liang, Y., et al. (2017). Rapid molecular profiling of defined cell types using viral TRAP. Cell Rep. *19*, 655–667.

Okaty, B.W., Freret, M.E., Rood, B.D., Brust, R.D., Hennessy, M.L., deBairos, D., Kim, J.C., Cook, M.N., and Dymecki, S.M. (2015). Multi-scale molecular deconstruction of the serotonin neuron system. Neuron *88*, 774–791.

Petreanu, L., Huber, D., Sobczyk, A., and Svoboda, K. (2007). Channelrhodopsin-2-assisted circuit mapping of long-range callosal projections. Nat. Neurosci. *10*, 663–668.

Petrovický, P., Kadlecová, O., and Masek, K. (1981). Mutual connections of the raphe system and hypothalamus in relation to fever. Brain Res. Bull. *7*, 131–149.

Pomeranz, L.E., Ekstrand, M.I., Latcha, K.N., Smith, G.A., Enquist, L.W., and Friedman, J.M. (2017). Gene expression profiling with Cre-conditional pseudorabies virus reveals a subset of midbrain neurons that participate in reward circuitry. J. Neurosci. *37*, 4128–4144.

Renier, N., Wu, Z., Simon, D.J., Yang, J., Ariel, P., and Tessier-Lavigne, M. (2014). iDISCO: a simple, rapid method to immunolabel large tissue samples for volume imaging. Cell *159*, 896–910.

Renier, N., Adams, E.L., Kirst, C., Wu, Z., Azevedo, R., Kohl, J., Autry, A.E., Kadiri, L., Umadevi Venkataraju, K., Zhou, Y., et al. (2016). Mapping of brain activity by automated volume analysis of immediate early genes. Cell *165*, 1789–1802.

Ribeiro, A.C., Ceccarini, G., Dupré, C., Friedman, J.M., Pfaff, D.W., and Mark, A.L. (2011). Contrasting effects of leptin on food anticipatory and total locomotor activity. PLoS ONE *6*, e23364.

Richardson-Jones, J.W., Craige, C.P., Guiard, B.P., Stephen, A., Metzger, K.L., Kung, H.F., Gardier, A.M., Dranovsky, A., David, D.J., Beck, S.G., et al. (2010). 5-HT1A autoreceptor levels determine vulnerability to stress and response to antidepressants. Neuron *65*, 40–52.

Schaeren-Wiemers, N., Schaefer, C., Valenzuela, D.M., Yancopoulos, G.D., and Schwab, M.E. (1995). Identification of new oligodendrocyte- and myelin-specific genes by a differential screening approach. J. Neurochem. *65*, 10–22.

Stachniak, T.J., Ghosh, A., and Sternson, S.M. (2014). Chemogenetic synaptic silencing of neural circuits localizes a hypothalamus→midbrain pathway for feeding behavior. Neuron *82*, 797–808.

Sternson, S.M., and Roth, B.L. (2014). Chemogenetic tools to interrogate brain functions. Annu. Rev. Neurosci. *37*, 387–407.

Veasey, S.C., Fornal, C.A., Metzler, C.W., and Jacobs, B.L. (1997). Single-unit responses of serotonergic dorsal raphe neurons to specific motor challenges in freely moving cats. Neuroscience *79*, 161–169.

Vertes, R.P. (1991). A PHA-L analysis of ascending projections of the dorsal raphe nucleus in the rat. J. Comp. Neurol. *313*, 643–668.

Vertes, R.P., and Kocsis, B. (1994). Projections of the dorsal raphe nucleus to the brainstem: PHA-L analysis in the rat. J. Comp. Neurol. *340*, 11–26.

Warden, M.R., Selimbeyoglu, A., Mirzabekov, J.J., Lo, M., Thompson, K.R., Kim, S.Y., Adhikari, A., Tye, K.M., Frank, L.M., and Deisseroth, K. (2012). A prefrontal cortex-brainstem neuronal projection that controls response to behavioural challenge. Nature *492*, 428–432.

Weissbourd, B., Ren, J., DeLoach, K.E., Guenthner, C.J., Miyamichi, K., and Luo, L. (2014). Presynaptic partners of dorsal raphe serotonergic and GABAergic neurons. Neuron *83*, 645–662.

Zhang, Y., Proenca, R., Maffei, M., Barone, M., Leopold, L., and Friedman, J.M. (1994). Positional cloning of the mouse obese gene and its human homologue. Nature *372*, 425–432.

STAR★METHODS

KEY RESOURCES TABLE

REAGENT or RESOURCE	SOURCE	IDENTIFIER
Antibodies		
Mouse monoclonal anti-GFP	Memorial-Sloan Kettering Monoclonal Antibody Facility	Htz-GFP-19F7 Htz-GFP-19C8
Chicken polyclonal anti-GFP	Abcam	Cat# ab13970; RRID: AB_300798
Rabbit polyclonal anti-c-Fos	Santa Cruz Biotechnology	Cat# sc-52; RRID: AB_2106783
Rabbit monoclonal anti-c-Fos	Cell Signaling	Cat# 2250S; RRID: AB_2247211
Chemicals, Peptides, and Recombinant Proteins		
Muscimol	Sigma-Aldrich	Cat# M1523-5MG
8-OH-DPAT	Sigma-Aldrich	Cat# H8520-25MG
Alpha-MSH	Sigma-Aldrich	Cat# M4135-5MG
3,36-PYY	Sigma-Aldrich	Cat# P220-500UG
NPY	Sigma-Aldrich	Cat# N5017-.5MG
Clozapine N-oxide	Sigma-Aldrich	Cat# C0832-5MG
Ghrelin	Tocris	Cat# 1465
Critical Commercial Assays		
SMARTer Ultra Low Input RNA for Illumina Sequencing	Clontech	Cat# 634822
Nextera XT DNA Sample Preparation Kit	Illumina	Cat# FC-131-1024
RNAscope Fluorescent Multiplex Reagent Kit	Advanced Cell Diagnostics	Cat# 320850
Deposited Data		
vTRAP RNA-seq raw and analyzed data	This paper	GEO: GSE87890
Experimental Models: Cell Lines		
293T	ATCC	Cat# CRL-3216
Experimental Models: Organisms/Strains		
Mouse: Vgat-IRES-Cre: *Slc32a1*$^{tm2(cre)Lowl}$/*J*	The Jackson Laboratory	016962
Mouse: VGLUT3-IRES-Cre	Lou et al., 2013	N/A
Mouse: Rosa26-LSL-EGFPL10a: B6.129S4-*Gt(ROSA)26Sor*$^{tm1(CAG-EGFP/Rpl10a,-birA)Wtp}$/*J*	The Jackson Laboratory	022367
Mouse: C57BL/6J	The Jackson Laboratory	000664
Mouse: ob/ob: B6.Cg-*Lep*^{ob}/J	The Jackson Laboratory	000632
Recombinant DNA		
AAV5-IV-GFPL10	This paper (packaged by UNC Vector Core)	N/A
AAV5-EF1a-DIO-hChR2(H134R)-EYFP	UNC Vector Core	N/A
AAV5-EF1a-DIO-EYFP	UNC Vector Core	N/A
AAV5-EF1a-DIO-eArch3.0-EYFP	UNC Vector Core	N/A
AAV5-EF1a-DIO-mCherry	UNC Vector Core	N/A
AAV5-hSyn-DIO-hM3D(Gq)-mCherry	UNC Vector Core	N/A
AAV5-hSyn-DIO-hM4D(Gi)-mCherry	UNC Vector Core	N/A
AAV5-EF1a-'Cre-out'-ChR2-EYFP	Gift of David Anderson (Cai et al., 2014)	N/A
Software and Algorithms		
GraphPad Prism 6.0	GraphPad	N/A
Python 3.5.1	Python	N/A
Cuffdiff v2.0.0	Cufflinks	N/A
Tophat v2.0.8b	Tophat	N/A

CONTACT FOR REAGENT AND RESOURCE SHARING

Further information and requests for reagents should be direct to and will be fulfilled by the Lead Contact, Jeffrey Friedman (friedj@rockefeller.edu).

EXPERIMENTAL MODEL AND SUBJECT DETAILS

All experiments were approved by The Rockefeller University Institutional Animal Care and Use Committee and were in accordance with the National Institutes of Health guidelines. Male mice (> 6 weeks old) were used for all studies. Mice were housed in a 12 hr light-dark cycle with ad libitum access to food and water, except for fasting assays. All mouse lines are in a wild-type (C57BL/6J) background. Genotypes/sources for mice used in the above studies are listed in the Key Resources Table. Male mice were used for all behavioral and molecular studies. Male and female mice were used for physiology studies, with no differences observed between sexes.

METHOD DETAILS

Viral Vectors

All viruses used in these studies were obtained from UNC Vector Core, Penn Vector Core, or were donated (see Key Resources Table for further information). For optogenetic studies, AAV5-EF1a-DIO-hChR2(H134R)-EYFP, AAV5-EF1a-DIO-eArch3.0-EYFP, or AAV5-EF1a-DIO-EYFP were used. For chemogenetic studies, AAV5-hSyn-DIO-hM3D(Gq)-mCherry, AAV5-hSyn-DIO-hM4D(Gi)-mCherry, or AAV5-hSyn-DIO-mCherry were used. For molecular profiling studies with vTRAP, custom AAV5-IV-GFPL10 was used (produced by the UNC Vector Core). For local CRACM studies, AAV5-EF1a-DIO-mCherry and AAV5-EF1a-'Cre-out'-ChR2-EYFP were used.

Construction of pAAV-IV-GFPL10

pAAV-IV-GFPL10 was generated by synthesizing a ~1.7 kb fragment with 3′ lox sites between anti-sense EGFP and sense Rpl10a coding sequence and 5′ AscI and 3′ EcoRI cut sites (Genewiz). The fragment was then subcloned into the plasmid pAAV-EF1a-DIO-ChR2-mCherry with AscI and EcoRI cut sites, replacing ChR2-mCherry and the 3′ lox sites. pAAV-IV-GFPL10 was then sent to the University of North Carolina Vector Core for AAV packaging with serotype 5.

Stereotaxic Surgery

Mice were anesthetized using isoflurane anesthesia, with induction at 3%–4% and maintenance at 1.5%–2%. Coordinates were identified using the Paxinos mouse brain atlas. For molecular profiling and chemogenetic studies, Vgat-IRES-Cre or VGLUT3-IRES-Cre mice were injected with 1.0 μL virus in the DRN using the following coordinates relative to lambda: (0 mm ML, 0 mm AP, −2.8 mm DV). For optogenetic studies, Cre-driver mice (VGLUT3-IRES-Cre, Vgat-IRES-Cre) were injected with 1.0 μL virus in the DRN (coordinates, relative to lambda: +0.8 mm ML, 0 mm AP, −3.0 mm DV:15°) followed by implantation of a fiber optic ferrule (Thor Labs) above the DRN (coordinates, relative to lambda: +0.8 mm ML, 0 mm AP, −2.4 mm DV:15°). For pharmacology studies, wild-type mice had cannulae (Plastics One) placed in the DRN (coordinates, relative to lambda: +0.8 mm ML, 0 mm AP, −3.0 mm DV:15°). The skin was closed with either sutures or a surgical clip. All DV coordinates listed are relative to the pial surface.

Cell Culture

HEK293T cells were transfected with pAAV-IV-GFPL10 with or without the plasmid pCMV-Cre (which constitutively expresses Cre recombinase). Live cells were then imaged using fluorescence microscopy. After imaging, cells were then trypsinized and split into two groups, for isolation of DNA and RNA, followed by downstream analyses.

Molecular Profiling

After stereotaxic surgery, mice were allowed to recover for approximately three weeks, allowing sufficient time for the incorporation of the GFPL10 fusion protein into the ribosome (Nectow et al., 2017). Briefly, mice were then sacrificed and the DRN and surrounding midbrain tissue was dissected out rapidly on ice. GFP immunoprecipitations (GFP IPs) were then performed according to previous protocols (Heiman et al., 2008). After performing GFP IPs, RNA was isolated using an Absolutely RNA Nanoprep Kit (Agilent), followed by RNA quantification and quality (as assessed by RIN value) on an Agilent 2100 Bioanalyzer. The QuantiTect Reverse Transcription Kit (QIAGEN) was then used for cDNA preparation, followed by Taqman qPCR and high-throughput RNA-seq. Transmembrane receptor genes were annotated using AmiGO 2 (term: transmembrane receptor activity'). Enrichment was calculated as GFP IP/Input.

RNA-seq

RNA-seq libraries were prepared using SMARTer Ultra Low RNA Kit (Clontech). Ten samples were sequenced (5 IPs paired with 5 Inputs). Each replicate was obtained through pooling of 4-5 mice. Sequencing was performed as 100 bp single-reads on an Illumina

HiSeq 2500 and evaluated using FASTQC. Reads were aligned to the mm9 build and Ensembl gene model (NCBIM37) using Tophat (tophat-2.0.8b). Cuffdiff (cufflinks-2.0.0) was used to determine differentially expressed genes for IP/Input and IP/IP comparisons. FPKM values are used for all plots.

Slice Electrophysiology

As previously described (Friedman et al., 2014), mice were perfused with artificial cerebrospinal fluid (aCSF) composed of (in mM): 128 NaCl, 3 KCl, 1.25 NaH_2PO_4, 10 D-glucose, 24 $NaHCO_3$, 2 $CaCl_2$, 2 $MgCl_2$ (oxygenated with 95% O_2 and 5% CO_2, pH 7.35, 295-305 mOsm). Acute brain slices were cut using a microslicer (Ted Pella) in 95% O_2 and 5% CO_2 saturated sucrose aCSF, which was derived by fully replacing NaCl with 254 mM sucrose. Slices were maintained in a holding chamber containing aCSF for 1 hr at 37°C. Slices containing the DRN were transferred into a recording chamber fitted with a constant flow rate of aCSF equilibrated with 95% O_2 and 5% CO_2 (2.5 ml/min) maintained at 35°C. Neurons were identified by their fluorescence and location under microscope. For spontaneous firing recordings, glass recording pipettes (6-8 MΩ) were filled with an internal solution composed of (in mM): 115 potassium gluconate, 20 KCl, 1.5 $MgCl_2$, 10 phosphocreatine, 10 HEPES, 2 magnesium ATP, and 0.5 GTP (pH 7.2, 285 mOsm). Cell-attached recordings were performed to record light-evoked firing activity in DRN neurons. Light-evoked activity was accomplished using optical fibers (Thor Labs), which were connected using an FC/PC adaptor to a 473 nm blue laser diode (Crystal Laser). An arbitrary waveform stimulator (Agilent Technologies) was used to generate light pulses. Partial access recordings were performed as previously described (Han et al., 2006) to measure the excitatory/inhibitory effects of a 2 min drug application on DRN^{Vgat} or DRN^{VGLUT3} neurons. Cells were classified as 'responding' if the drug had a $\geq$ 10% effect on cells (Drug/Base) and returned back toward baseline during Wash. For light-evoked IPSCs, glass recording pipettes (2.5-3.5 MΩ) were filled with (in mM):120 CsCl, 10 Phosphocreatine-Na, 10 HEPES, 10 EGTA, 2 magnesium ATP, and 0.3 GTP-Tris (pH 7.2, 285 mOsm) to perform whole cell recordings. Kynurenic acid (1mM) was added into aCSF to block NMDA and AMPA/kainate receptor-mediated excitatory postsynaptic responses. Evoked IPSCs were obtained at a holding potential of −65 mV and confirmed to be γ-aminobutyric acid (GABA)-mediated in each recording by adding 100 μM picrotoxin. Data acquisition was collected using a Multiclamp 700B, a Digidata 1440A digitizer and pClamp 10.2 (Molecular Devices).

In Vivo Photostimulation

For all optical activation studies, mice received blue light laser stimulation (473 nm, OEM Lasers/OptoEngine) of approximately 10 mW with a 10-ms pulse width (see text for frequency). For optical inhibition studies, mice received constant green light stimulation (532 nm, OEM Lasers/OptoEngine) of approximately 10 mW. Stimulation paradigms were programmed into an arbitrary waveform generator (Agilent). Mice were handled at least three days prior to performing behavior. DRN^{Vgat} and DRN^{VGLUT3} neurons were stimulated as indicated in the text.

Food Intake Assay for Optogenetic Studies

The food intake assay was performed in the home cage. A weigh boat containing standard mouse chow was placed in the corner of the home cage, and food intake was measured over three 20 min epochs (Laser Off, Laser On, Laser Off), respectively. During the Laser On epoch, mice received continuous optogenetic stimulation (frequency is defined in the text). In food deprivation studies, mice were food deprived through their entire previous dark cycle.

Food Intake Assay for Chemogenetic Studies

The food intake assays were performed in the home cage. Mice were given ad libitum access to food prior to, during, and after the assay. Measurement of food intake was made at 1, 2, and 4 hr post i.p. injection of CNO. For *ob/ob* weight loss studies, mice were injected twice per day with either vehicle or CNO. All CNO injections were at a concentration of 0.5-1 mg/kg.

Food Intake Assay for Pharmacology Studies

The food intake assays were performed in the home cage, where mice were given ad libitum access to food prior to, during, and after the assay. Measurements of food intake were made at 1, 2, 4, and 8 hr post injection/infusion. Pharmacology infusions were performed using a pump (Harvard Apparatus) and syringes (Hamilton), with an infusion rate of 0.1 μl/min, with a total injection volume of 0.5 μL for all drugs.

Open Field Test for Optogenetic Studies

The open field test (OFT) was performed in three 5 min epochs (Laser Off, Laser On, Laser Off), respectively. During the Laser On epoch, mice received continuous optogenetic stimulation (frequency is defined in the text).

iDISCO+ Brain Clearing

Mice were perfused transcardially with PBS followed by 4% PFA. After a 24 hr post-fixing period, immunolabeling and whole-brain clearing and immunolabeling was performed, followed by analysis using ClearMap (Renier et al., 2016). A LaVision Ultramiscrope was used for light sheet imaging of cleared brains.

QUANTIFICATION AND STATISTICAL ANALYSIS

Statistical parameters reported in the Figures and Figure Legends are the following: sample size (n = number of animals or samples per group), definition of center, dispersion, precision measures, statistical test used, and statistical significance. All data are displayed as mean ± SEM. Significance was defined as $p < 0.05$. Significance annotations are: *$p < 0.05$, **$p < 0.01$, ***$p < 0.001$, ****$p < 0.0001$. Mice were randomized into control or treatment groups. Control mice were age-matched littermate controls where possible. All statistics and data analysis were performed using GraphPad Prism, MATLAB, R, or Python. For RNA-seq, transcript abundance and differential expression were performed using cufflinks.

DATA AND SOFTWARE AVAILABILITY

Data Resources

The accession number for vTRAP RNA-seq data reported in this paper is GEO: GSE87890 and can be found at: https://www.ncbi.nlm.nih.gov/geo/query/acc.cgi?acc=GSE87890.

Cell

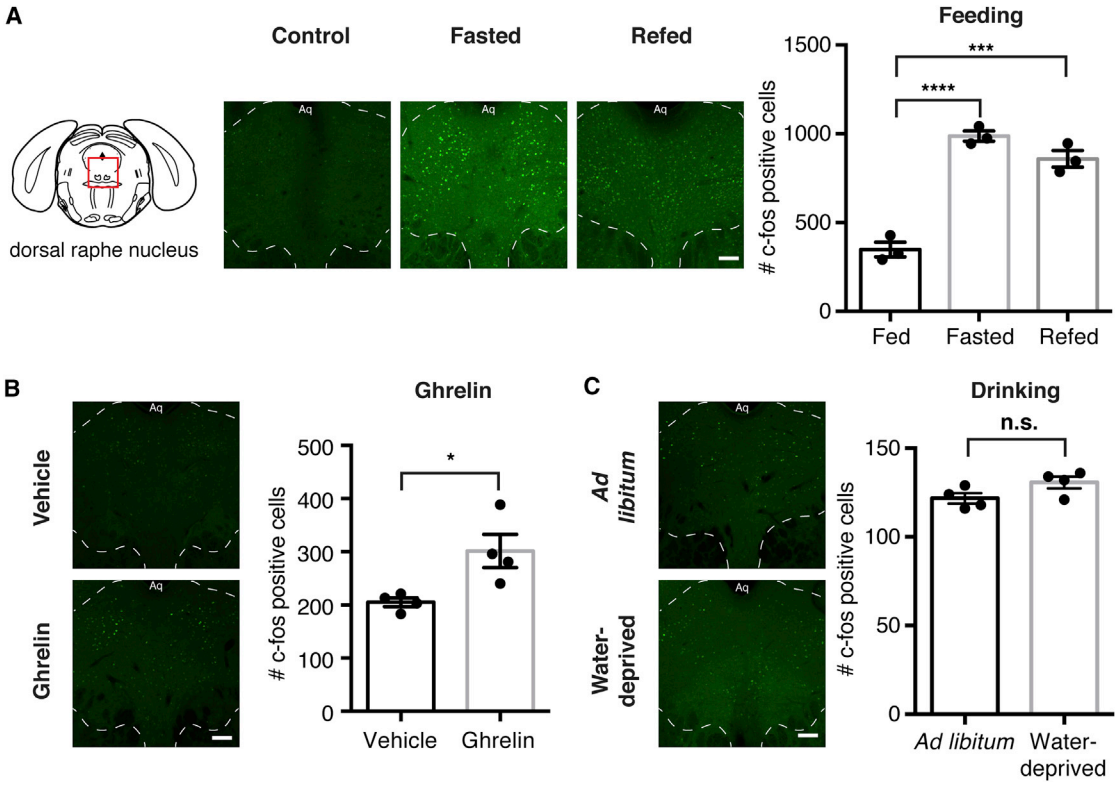

Figure S1. DRN^{Vgat} and DRN^{VGLUT3} Neurons Are Differentially Activated by Fasted and Re-fed States, Related to Figure 1

(A) Immunohistochemistry for Fos. DRN neurons are activated after an overnight fast ('Fasted'), as well as after a 2 hr re-feeding after an overnight fast ('Refed'). One-way ANOVA (Treatment: $p < 0.0001$; $n = 3$ mice per group).

(B) DRN neurons are activated by i.p. injection of orexigenic hormone ghrelin (400 μg/kg). Unpaired t test ($n = 4$ mice per group).

(C) DRN neurons are not activated by overnight water deprivation. Unpaired t test ($n = 4$ mice per group).

All scale bars, 100 μm. n.s. not significant, *$p < 0.05$, ***$p < 0.001$, ****$p < 0.0001$. Data are presented as mean ± SEM.

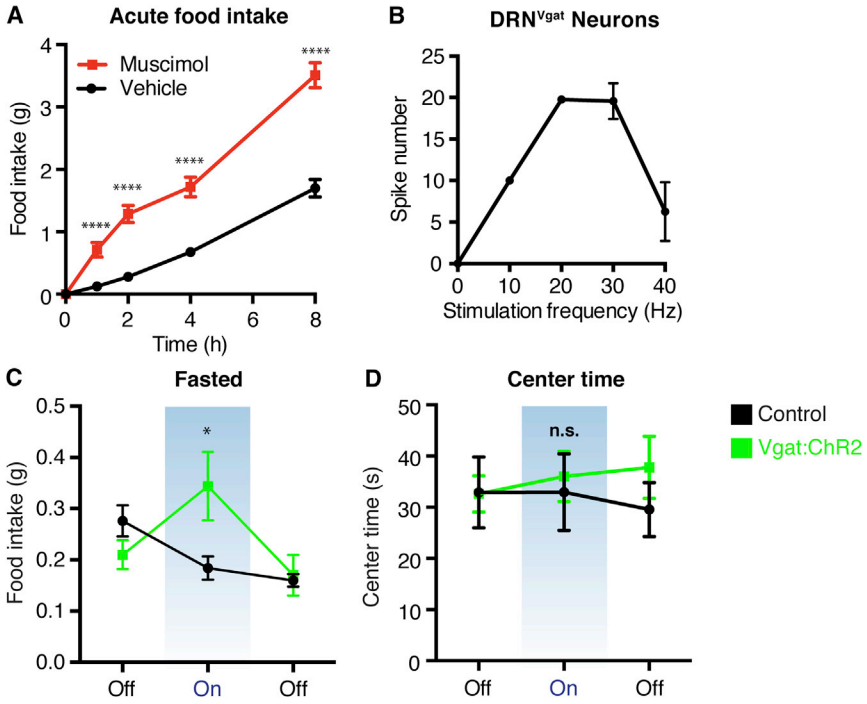

Figure S2. Modulation of DRN^{Vgat} Neurons, Related to Figure 2

(A) Selective $GABA_A$ receptor agonist muscimol (0.5 μl, 0.5 μg/μl), or vehicle, is infused into the DRN of wild-type mice fed ad libitum. Muscimol significantly increases food intake relative to saline treatment. Two-way RM-ANOVA (Treatment: $p < 0.0001$; $n = 9$ mice per group).

(B) DRN^{Vgat} neurons transduced with ChR2(H134R)-EYFP can follow 20 Hz photostimulation with high fidelity.

(C) Photoactivation of DRN^{Vgat} neurons after an overnight fast induces significant food intake. Two-way ANOVA comparing treated and control groups ($n = 5$ mice per group).

(D) Optical stimulation of DRN^{Vgat} neurons has no effect on center time in the open field test. Two-way ANOVA comparing treated and control groups ($n = 7$-10 mice per group).

n.s. not significant, *$p < 0.05$, ****$p < 0.0001$. Data are presented as mean ± SEM.

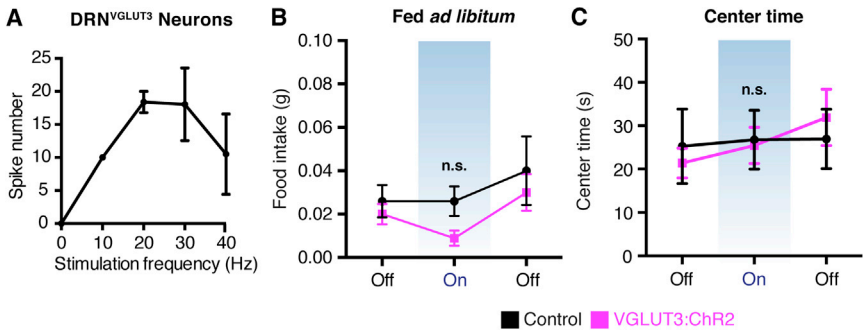

Figure S3. Modulation of DRN^{VGLUT3} Neurons, Related to Figure 3

(A) DRN^{VGLUT3} neurons transduced with ChR2(H134R)-EYFP can follow 10 Hz photostimulation with high fidelity.

(B) Optical stimulation of DRN^{VGLUT3} neurons in mice fed ad libitum does not significantly effect food intake. Two-way ANOVA comparing treated and control groups (n = 5-9 mice per group).

(C) Optical activation of DRN^{VGLUT3} neurons has no effect on center time in the open field test. Two-way ANOVA comparing treated and control groups (n = 24 mice per group).

n.s. not significant. Data are presented as mean ± SEM.

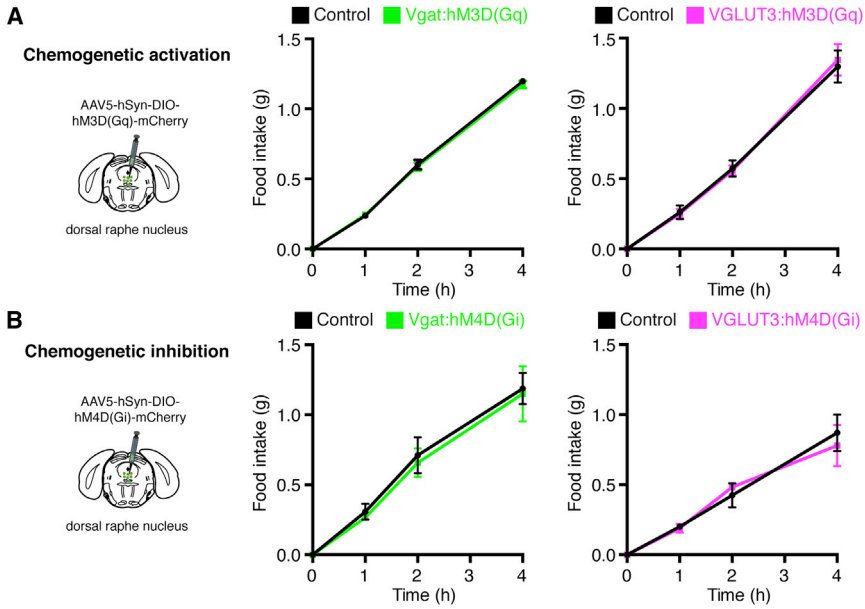

Figure S4. Saline Control Injections for Chemogenetic Modulation of DRN^{Vgat} and DRN^{VGLUT3} Neurons, Related to Figure 4

(A and B) Control (vehicle) injections for excitatory (A) and inhibitory (B) DREADD studies. Saline injections have no effect on food intake ($p > 0.05$ for all treatments). Two-way ANOVA comparing treated and control mice (n = 4-7 mice per group).

Data are presented as mean ± SEM.

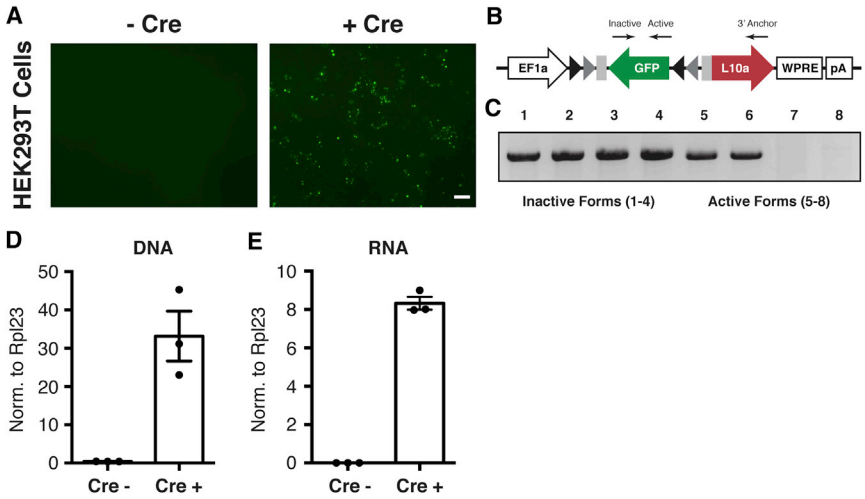

Figure S5. Development and Validation of pAAV-IV-GFPL10, Related to Figure 6

(A) Live cell imaging of HEK293T cells transfected with pAAV-IV-GFPL10 plasmid in the presence (right) or absence (left) of a Cre recombinase-expressing plasmid. Expression of GFP is only observed in the co-presence of pAAV-IV-GFPL10 and the Cre-expressing plasmid.

(B) AAV-IV-GFPL10 schema with annotation of primer sites to identify 'inactivated' and 'activated' variants.

(C) PCR of DNA made from transfected HEK293T cell lysate from (A). Activated form of GFPL10 is detected only in the Cre-positive treatments, whereas the inactivated form of GFPL10 is detected in both treatments. Columns 1-4: Inactive GFPL10 (+ Cre: 1-2, - Cre: 3-4); Columns 5-8: Active GFPL10 (+ Cre: 5-6, - Cre: 7-8). DNA ladder is omitted.

(D and E) qPCR for activated form of GFPL10 at the level of DNA ($p < 0.01$, D) and RNA ($p < 0.0001$, E). Unpaired t test.

Scale bar, 100 μm. Data are presented as mean ± SEM.

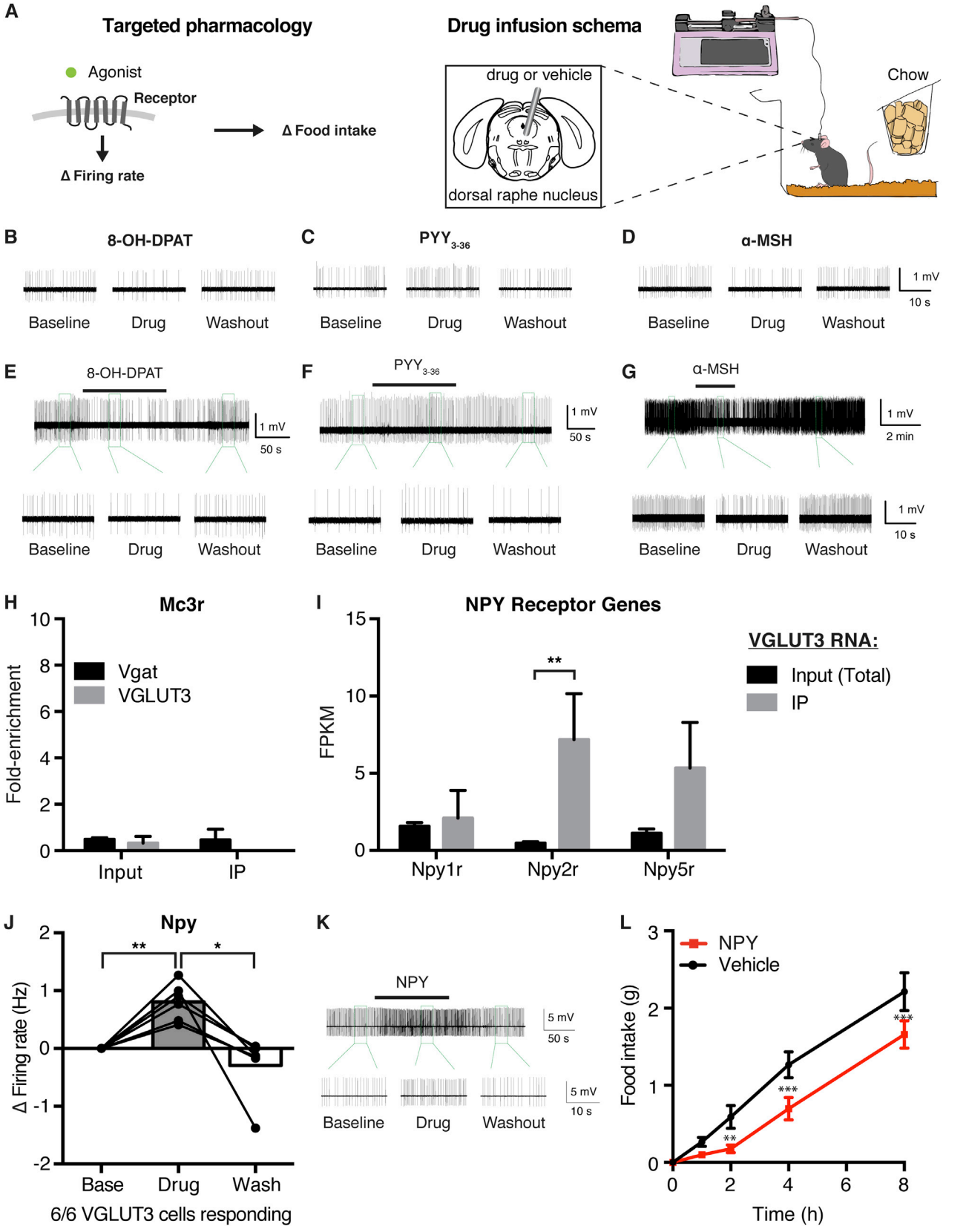

(legend on next page)

Figure S6. Pharmacology and Molecular Profiling in the Dorsal Raphe Nucleus, Related to Figure 7

(A) Schemata for targeted pharmacology of neurons to influence feeding behavior using a priori knowledge of cell membrane receptor composition (left), and drug infusion into the DRN to influence feeding behavior (right). Mice fed ad libitum are initially infused with drug, followed by an 8 hr post-infusion feeding session.

(B–D) Magnified responses of DRN^{VGLUT3} neurons to 8-OH-DPAT (B) and PYY_{3-36} (C) and DRN^{Vgat} neurons to α-MSH (D).

(E) Responses of DRN^{VGLUT3} neurons to 8-OH-DPAT in the presence of synaptic blockers kynurenic acid (KYN) and picrotoxin (PTX). 5/5 neurons were inhibited by 8-OH-DPAT.

(F) Responses of DRN^{VGLUT3} neurons to PYY_{3-36} in the presence of KYN and PTX. 4/4 neurons were activated by PYY_{3-36}.

(G) Responses of DRN^{Vgat} neurons to α-MSH in the presence of KYN and PTX. Cellular responses: 6/10 neurons were inhibited, 2/10 neurons were activated, 2/10 neurons had no effect.

(H) Melanocortin 3 receptor (*Mc3r*) is depleted from both DRN^{Vgat} and DRN^{VGLUT3} neurons.

(I) Enrichment of NPY receptors in DRN^{VGLUT3} neurons. Only Npy2r is significantly enriched in DRN^{VGLUT3} neurons. Paired t test comparing Input and IP.

(J) DRN^{VGLUT3} neurons are activated by Neuropeptide Y (NPY; 1 μM). 6/6 neurons responded from n = 3 mice. One-way RM-ANOVA (Treatment: $p < 0.01$).

(K) Sample trace of a DRN^{VGLUT3} neuron responding to NPY.

(L) Local infusion of NPY (0.5 μl, 156 pmol/μl) into the DRN suppresses food intake up to 8 hr after initial injection. n = 7, two-way RM-ANOVA (Treatment: $p < 0.05$).

*$p < 0.05$, **$p < 0.01$, ***$p < 0.001$. Data are presented as mean ± SEM.